Effect of DHODH Deficiency on p53 Expression and Osteoblast Differentiaion in Miller's Syndrome Mouse Model

Preliminary RHEP

Urwah Nawaz

a1654797

Declaration:

This work does not contain any material written by another person, except where due reference is given in the text, and the work has not been presented previously as a component of any other academic course.

Word Count: 2494

Word count includes titles and figure legends, but excludes in-text references, appendices and acknowledgements

Hypothesis

Dhodh deficiency causes an increase in p53 levels which subsequently repress Osterix/Sp7 during embryonic development in Miller's syndrome mouse model.

1 Background

The developments of the face and limbs are intricate processes tightly regulated by signalling pathways and transcription factors (TFs) (Karsenty et al., 2009). Misregulation of these processes in the developing embryo leads to skeletal anomalies affecting approximately 1 in 3000 births (Stoll et al., 1989). Miller's syndrome (MS) (OMIM:263750) is a rare autosomal recessive congenital disorder characterised by craniofacial and postaxial limb abnormalities (Miller et al., 1979). These abnormalities include severe micrognathia, cleft lip and/or palate, and hypoplasia or aplasia of the posterior elements of the limbs. The mechanisms underlying the aetiology of MS are incompletely understood.

1.1 Cause of Miller's syndrome

MS is caused by compound heterozygous missense mutations in the protein coding regions of the *DHODH* gene (Ng et al., 2010). A total of 14 different mutations in *DHODH* have been reported (Ng et al., 2010; Rainger et al., 2012). Each patient tends to carry a different combination of mutations, which dictates the severity of the MS phenotype.

DHODH gene contains nine exons that encode a 43-kDa protein dehydroorotate dehydrogenase (DHODH). DHODH is a key enzyme in the *de novo* pyrimidine synthesis and localises in the inner mitochondrial membrane. DHODH catalyses the oxidation of dehydroorate to orotate, linking it to the mitochondrial respiratory chain (MRC) by using ubiquinone as a substrate (Fang et al., 2013). *In vivo* and *in vitro* assays revealed an overall reduced enzymatic DHODH activity from 11 MS associated alleles (Rainger et al., 2012). Three disease-associated

missense mutations were further evaluated, revealing reduced protein stability (G202A and R346W) or impairment in the substrate-induced enzymatic activity (R135C) (Fang et al., 2012). These mutants retained their normal mitochondrial localisation. This implies that affected individuals have a deficiency of *de novo* pyrimidine synthesis. No individual has been identified with both alleles showing severe loss-of-function (LOF) (Rainger et al., 2012). Consistently, an upper and lower threshold for DHODH activity has been established, where greater than 50% activity results in a normal phenotype, but insufficient activity leads to embryonic lethality (Rainger et al., 2012). The mechanisms by which DHODH deficiency causes the MS phenotype are not clear.

1.2 DHODH deficiency and p53 activation

Selective inhibition of pyrimidine biosynthesis is used as a therapeutic approach to treat various cancers and autoimmune disorders (Ren et al., 2017; Liu et al., 2017; Leban and Vitt, 2011). Leflunomide, converted to the active metabolite, Teriflunomide, reduces *de novo* pyrimidine biosynthesis by selectively inhibiting DHODH (Figure 1).

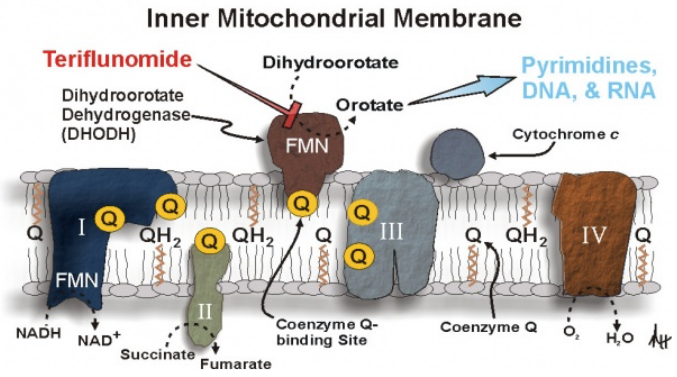

Figure 1: Teriflunomide inhibits DHODH thereby causing an impairment in the pyrimidine nucleotide pool, and defective MRC complex III. Reproduced from Vélez et al. (2013)

Cancer cell-lines treated with leflunomide show that DHODH inhibition leads to a depletion in the pyrimidine nucleotide pool, and generation of reactive oxygen species (ROS), via mitochondrial dysfunction. These effects have contributed to an increase in p53 levels, which

inhibit cell proliferation, induce cell-cycle arrest, and cause p53 dependent apoptosis in human cancer-cell lines (Linke et al., 1996; Khutornenko et al., 2010; Hail et al., 2012; Fairus et al., 2017).

A common feature among several craniofacial abnormalities is p53 activation however the mechanisms involved are not completely elucidated (Jones et al., 2008; Barlow et al., 2010; Boultwood et al., 2012; Sakai et al., 2016). Mutations in the *Tcof1* gene in Treacher Collins Syndrome (TCS), lead to an increase p53 levels in the neuroepithelium of the TCS mouse model. Knock-out (KO) and pharmacological inhibition of p53 ameliorates the craniofacial phenotype in the TCS mouse model (Jones et al., 2008; Sakai et al., 2016). Similarly, p53 stabilization in cranial neural crest cells (CNCC) leads to craniofacial defects in mouse and chick embryos, indicating that p53 coordinates CNCC growth by affecting cell cycle gene expression and proliferation at discrete developmental stages (Rinon et al., 2011). It is possible that DHODH deficiency causes an up-regulation in p53 that lead to the defects observed in MS.

While evidence supports that DHODH deficiency leads to an increase of p53, some studies have shown conflicting results. Previously, siRNA-mediated DHODH depletion in HeLa cells showed no difference in p53 levels (Fang et al., 2013). Additionally, treatment with leflunomide in null-p53 mutant zebrafish led to a decrease in migrating neural crest cells (White et al., 2011), suggesting that DHODH may function in a p53 independent manner. However, these results could be attributed to tissue-specific variation and thus the involvement of p53 in MS warrants further investigation.

1.3 Craniofacial and Limb Development

MS diagnose is associated with defective craniofacial and limb development. Internal malformations are uncommon in MS patients (Rainger et al., 2012), implying that the developmental pathways affected in MS disrupt cartilage and bone development. Consistently, the mouse orthologue,

Dhodh showed spatio-temporal expression during E10.5 (Embryonic day post coitum) in craniofacial region, hindlimbs and forelimbs (Rainger et al., 2012).

The differentiation of osteoblasts from the mesenchymal precursors is controlled by a hierarchy of TFs including Runx2 and Osterix (or SP7) (Karsenty et al., 2009). Conditional inactivation of Osx/SP7 in CNCC has resulted in defective craniofacial bone development in mice (Baek et al., 2013). Additionally, a human patient with a homozygous mutation in Osx/SP7 displayed craniofacial and limb bone deformities (Lapunzina et al., 2010) inclduing midface hypoplasia, micrognathia, and asymmetry of the limbs. These phenotypes overlap with MS phenotype.

p53 exerts a repressive effect on osteoblast differentiation and bone development (Ohyama et al., 1997; Wang et al., 2006). In osteosarcoma development, LOF of p53 causes abnormal osteogenesis, and up-regulation of Runx2 and Osx/SP7 (Berman et al., 2008). Similarly, p53 is able to directly repress Osx causing a decrease in osteoblast differentiation (Artigas et al., 2017). Thus, the p53-mediated inhibition of Osx might have implications in bone formation under pathological conditions during embryonic development.

In MC3T3-E1 cells, depletion of DHODH activity decreases osteogenic gene expression. Expression and protein levels of p53 increased in this study, although the relationship between p53 and osteoblast differentiation was not explored. MC3T3-E1 cells contain Osx/SP7 (Tian et al., 2012). *Osx* mRNA levels in mice show significant up-regulation between E11.5 and E13.5, subsequent to the increased *Dhodh* expression at E10.5 (Gao et al., 2004; Kaback et al., 2008; Rainger et al., 2012). It is possible that one of the mechanisms by which DHODH deficiency (as a result of the mutations) leads to the MS phenotype is by increasing p53 levels which subsequently represses Osx/SP7 (Figure 2).

2 Experimental Overview

2.1 Proposed model

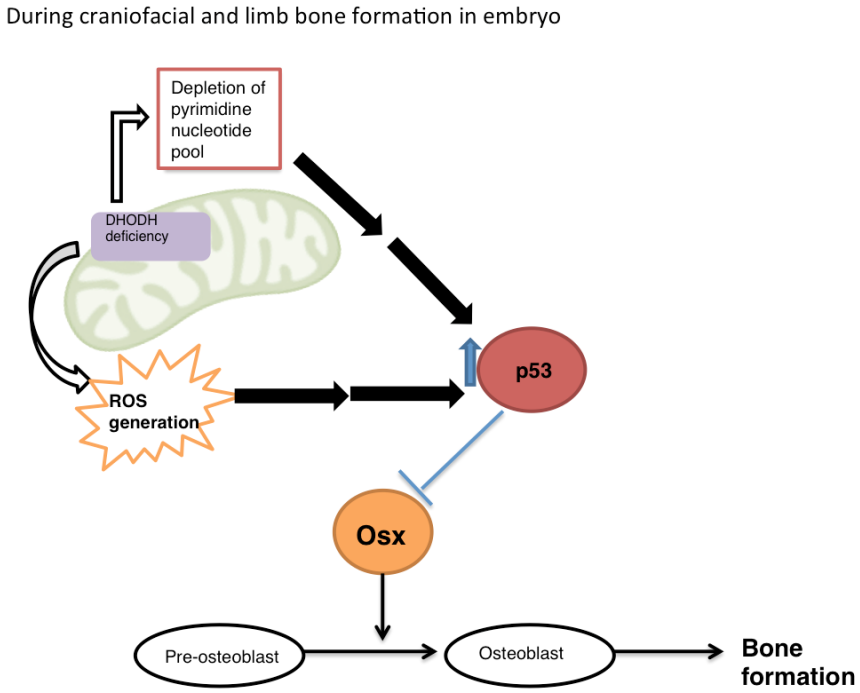

Figure 2: Illustration of the proposed model. DHODH mutations cause Dhodh deficiency leading to mitochondrial dysnfuntion and depletion of pyrimidine nucleotide pool. As a result, p53 levels are increased and subsequently repress Osterix/SP7 during embryonic development

2.2 Experimental Aims

Aim 1: To generate a mouse model system for Miller's Syndrome using CRISPR-Cas9

Aim 2: To determine if p53 levels are increased during craniofacial and limb development due to Dhodh deficiency by using mRNA and protein quantification techniques

Aim 3: To determine if Osx/SP7 is being repressed due to increased p53 levels via Dhodh deficiency using quantitative Real Time-PCR and Proximity Ligation Assay

2.3 Experimental Plan

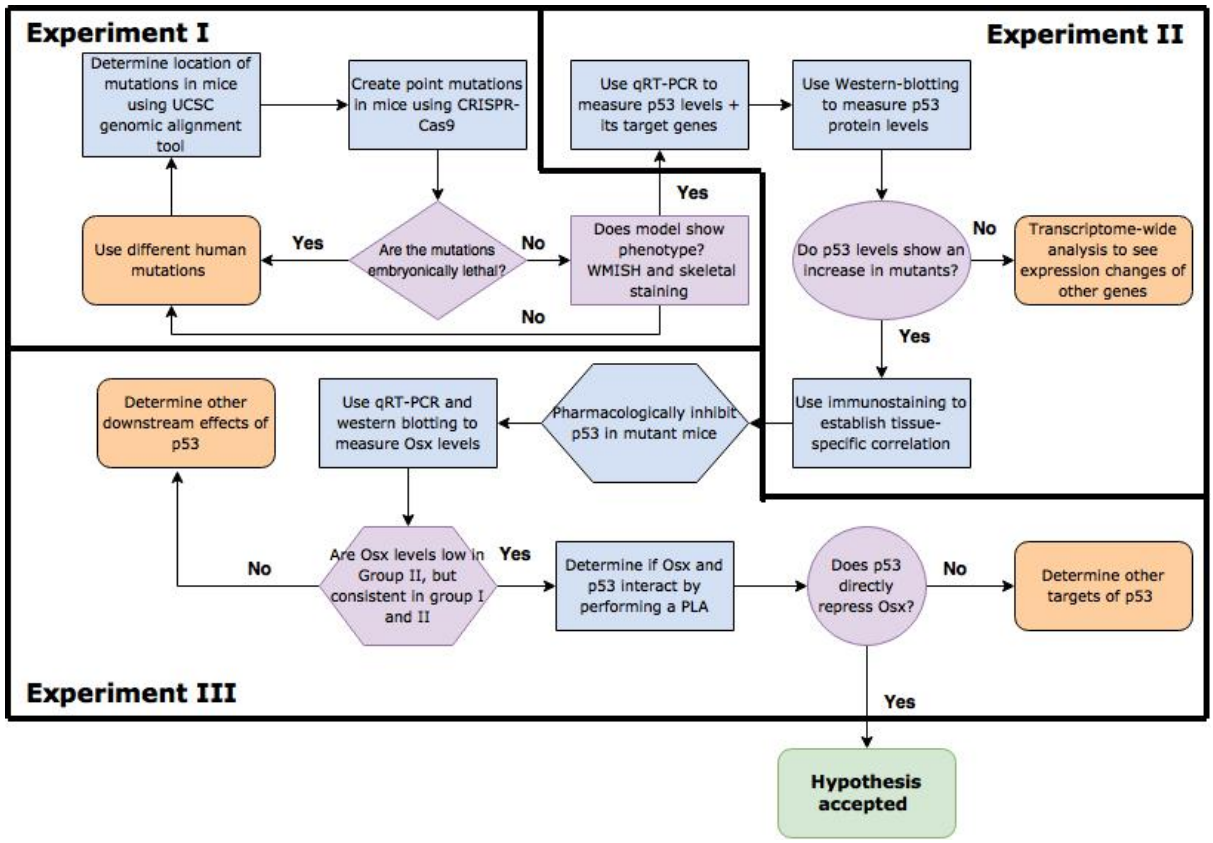

Figure 3: Flowchart and Summary of Experimental plan. Blue: Experiments; Purpler: Experimental questions; and Orange: Alternative experiments if desired results not obtained.

2.4 Controls for the experiment

Table 1: Mice and controls for this study

Mice	Description	Treatment	Group
Wildtype mouse (WT)	C57BL/6J mice embryos	Control	I
Dhodh mutant mice	Mice embryos maintained on C57BL/6J background	Mice generated using CRISPR/Cas9 as described in Experiment 1	II
Dhodh mutant mice embryos with p53 inhibitor	Mice embryos maintained on C57BL/6J background	Mice treated with pifithrin-α as described in Experiment III	III

The embryos will be obtained by timed mating; the morning of the vaginal plug is considered to be E0.5. Embryos will be collected as described by Piliszek et al. (2011) at stages E9.5,

E10,5, E11.5, E12.5, E13.5 and E14.5. Each experiment specifies at what stage the embryos are collected. Three embryos from each group at each specific stage will be used for each experiment, unless otherwise specified.

3 Experiment I: Generation of mouse model for Miller's syndrome

3.1 Proposed Experiments

CRISPR-Cas9 will be used to introduce the human missense mutations p.R135C and p.E52G will be introduced into mice *Dhodh*. USCS genomic tool will identify the corresponding mutations in mice (Kuhn et al., 2012). Guide RNA (gRNAs) and single-stranded oligodeoxynucleotides (ssODNs) will be generated as previously detailed (Inui et al., 2014) and examples are shown in Table 3. Potential off-target sites will be predicted using the algorithm determined by Zhang-Laboratories (2018). Examples of gRNAs and ssODNs are listed in Table 2. Off-target

Table 2: Examples of gRNAs and ssODNs generated for base substitutions using CRISPR design tool by Zhang lab

Mutation	gRNAs	ssODNs	Quality Score of gRNA(%)	Off-target score of gRNAs
155A>G;p.E52G	5′ TTGATCCAGAGTCGGCGCACCGG 3′	5' TTTCTACGCCGA GTACCTGATGCCG GCTCTGCAGAGA CTGCTTGATCCAG **G** GTCGGCGCACC GGCTAGCTGTTCG AGTCATCTCCCTG GGGCTCCTTC 3′	97	0.3
403C>T;pR135C	5′ CCGAGTATTCCGTCTCCCTGAGG 3′	5′GTTGAGGTGGGAAG TGTGACTCCCCAGCCT CAGGAAGGAAACCCCA GGCCCCGAGTATTC**T**GT CTCCCTGAGGACCAAGC TGTTATTAACAGG 3′	80	0.5

hit scores are computed as 100% minus a weighted sum of off-target hit-scores in the target genome taking into account the number of mismatches. The gRNA and ssODNs mixed in a hCas9 vector mRNA will be injected into mouse zygotes and transferred to pseudo-pregnant females as described before (Inui et al., 2014; Kato et al., 2013; Takada et al., 2013). Genomic DNA will be obtained and assessed for the presence of mutations in the *Dhodh* gene. Mice harbouring mutant alleles will be bred to obtain $Dhodh^{E52G/R135C}$ pups. Point mutations will be confirmed by sequence analysis of genomic DNA extracted from individual embryos as described (Inui et al., 2014). For skeletal staining, the skeleton of E17.5 $Dhodh^{E52G/R135C}$ pups will be fixed in 99% ethanol and stained for bone and cartilage as described (Baek et al., 2014). In subsequent experiments, $Dhodh^{E52G/R135C}$ mice will be known as Group II.

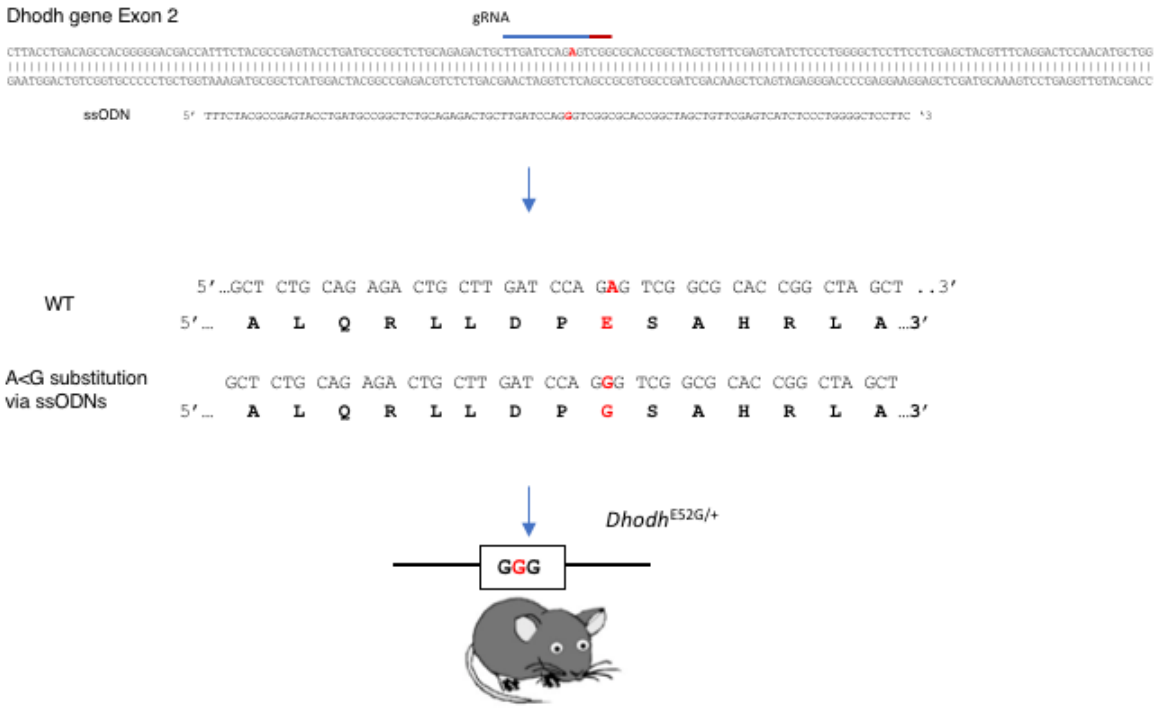

Figure 4: Schematic illustration of showing the locations of a gRNA and ssODN used to generate the 155A<G base substitution, along with the exon 2 of *Dhodh* gene, and expected genotype of the mouse. Blue bar indicates target of the gRNA with the red bar highlighting the PAM sequence. Red letters indicate the substitution target site in the *Dhodh* locus and corresponding mismatched nucleotides in the ssODNs

Whole-mount *in situ* hybridisation (WMISH) will be performed and fluorescence levels

will be quantified as described before (Rainger et al., 2012) with probes specific for *Dhodh* on Group I and Group II at E10.5.

3.2 Possible outcomes and interpretation

Previously, leflunomide had been able to replicate the MS phenotype in zebrafish or mice (White et al., 2011; Fukushima et al., 2009). However, this approach was limited by the off-target effects of leflunomide, such as inhibiting tyrosine kinases. (Fukushima et al., 2009). Therefore, by using CRISPR-Cas9, the mutations found in MS patients can be replicated in a mouse model, and provide a better understanding of DHODH deficiency in the developing embryo. The human point mutations p.E52G and p.R135C selected because clinical details for the human carrier of these mutations had features most typical for the syndrome (Rainger et al., 2012). Additionally, previous *in vitro* analysis revealed that the residual activity for R135C is >50%, whereas the activity for E52G is <10% which gives a combination of a moderate LOF and a severe LOF allele, consistent with the threshold activity of DHODH (Rainger et al., 2012).

By using WMISH, expression levels of *Dhodh* can be compared between WT and mutant. Lower *Dhodh* expression should be expected in Group II. Expected phenotype characteristics include: cleft palate, mandibular micrognathia in the craniofacial region, and anomaly of limb and digits, a short and/or tinted tail (Fukushima et al., 2009). These will be analysed using skeletal staining. Normal Mendelian frequencies are expected: $Dhodh^{E52G/R135C}$, $Dhodh^{+/R135C}$ and $Dhodh^{+/+}$ pups. As reported previously on Mouse-Phenotype (2018), global deletion of *Dhodh* gene results in embryonic lethality, so mice homozygous for E52G will not be expected to survive.

It is possible that the point mutations will not result in the desired phenotype, or cause embryonic lethality. If this occurs, different human *DHODH* mutations (Appendix A) should be generated in mice using the same strategy.

4 Experiment II: Investigating p53 levels in Miller's syndrome mouse model

Hypothesis: p53 levels will show a spatiotemporal increase after E10.5 during mouse embryonic development.

4.1 Proposed Experiments

quantitative Real Time-PCR

Trp53, *Ccng1* , *Trp53inp1*, *Pmaip1*, *Perp* and *Wig1* will be analysed using qRT-PCR. Total RNA will be extracted from E9.5 through E12.5 Group I and II embryos using RNeasy Mini Protocol for Isolation of Total RNA from Animal Tissues (Qiagen), following the manufacturer's instructions. cDNA will be synthesised using a reverse transcription kit (Qiagen). *Gadph* will serve as a house-keeping gene. Quantitative analysis of each gene product will performed via RT-PCR using specific primers. All measurements will be performed in triplicates.

Western blotting

p53 proteins will be extracted from E9.5 through E12.5 Group I and II embryos, separated using SDS-PAGE. p53 protein will be detected by using monoclonal antibody to p53. α-tubulin, detected using monoclonal antibody to α-tubulin mouse ascites fluid, will be used for normalization.

Immunohistochemistry

Immunostaining of Group I and II will be done for E9.5-E12.5. A specific antibody to p53 will be used. All sections will be counter-stained with DAPI. Whole-mount immunohistochemistry and fluorescence quantification will be performed as previously described by Jones et al. (2008) and Ueda et al. (2006).

4.2 Possible outcomes and interpretation

Analysing samples over a series of embryonic stages will allow p53 quantification before and after E10.5. Additionally, we can determine if the levels stay stabilised over several stages. Protein and mRNA levels are measured as mRNA levels are not normally indicative of protein levels (de Sousa Abreu et al., 2009). *Ccng1*, *Trp53inp1*, *Pmaip1*, *Perp* and *Wig1* are all recognized targets of p53-dependent transcription (Levine, 1997), therefore any upregulation in these would indicate an increase of p53 levels. Immunostaining will provide a tissue-specific correlation between increased p53 levels and the tissues affected in MS (Jones et al., 2008). It is expected that an increase p53 protein will be observed in craniofacial, hindlimbs and forelimbs regions.

If significant up-regulation is observed in p53 markers, or in p53 protein after E10.5, it could indicate that Dhodh deficiency leads to p53 activation. Alternatively, if no significant up-regulation is observed, then a transcriptome wide-analysis of Group II can be undertaken to examine expression level changes throughout the developing embryo in Dhodh deficient conditions .

5 Experiment III: Investigation of Osx/SP7 repression due to increased levels of p53 via Dhodh deficiency

Hypothesis: Osx/SP7 will be respressed in *Dhodh* mutant mice due to increased p53 levels

5.1 Proposed Experiments

Pharmacological Inhibition of p53 in Mutant mice

Mutant female mice, bred with mutant male mice to generate $Dhodh^{E52G/R135C}$ heterozygotes as described in Expeirment 1, will be treated with pifithrin-α (Alexis Biochemicals) as described before (Jones et al., 2008).

qRT-PCR and Western-blotting

To investigate if *Osx* expression is influenced by Dhodh deficiency, qRT-PCR will be performed on Groups I-III as in Experiment 2 at E11.5-E13.5. The genes *Runx2*, *Osx* and early osteoblast differentiation markers *BSP, osteonectin* and *osteopontin* will be analysed using specific primers. Osx will also be analysed in protein by western-blotting, as in Experiment 2. Protein will be extracted from E11.5-E13.5 embryos from Groups I-III.

Proximity Ligation Assay (PLA)

An immunofluorescent staining of pre-implantation embryos (Group II) will be performed as described. Briefly, specific antibodies for p53 and Osx will be used. The Duolink *in situ* PLA kit will be used according to the manufacturers protocol. Imaging and fluorescence intensity quantification will be performed using ImageJ2 (Rueden et al., 2017). PLA quantification will be performed using Blobfinder v3.2 (Allalou and Wählby, 2009).

5.2 Possible outcomes and interpretations

Analysis of *Osx* and osteoblast marker genes (Tang et al., 2011) will allow us to determine if their expression is being influenced by Dhodh deficiency. Group III will allow us to determine if these expression changes are due to high p53 levels. It is expected that the osteoblast genes will have significantly lower expression in group II, and identical expression in Group I and Group III. PLA will be performed in mutant mice to see if Osx physically interacts with p53. PLA allows to visualise protein-protein interaction *in situ*, by fluorescently labelling of sites in which the proteins of interest are in close proximity (<40 nm) (Thymiakou and Episkopou, 2011).

Runx2 acts upstream of Osx and will be used as a negative control. If *Runx2* levels also show down-regulation, it could imply that p53 either represses Runx2 (Ozaki et al., 2013), or works by other mechanisms, such as cell-cycle arrest or apoptosis, which contribute to the decreased *Osx* expression levels. In these cases, PLA specific for Runx2, TUNEL assays and/or cell cycle analyses by flow cytometry should be performed. Alternatively, if no change in Osx and osteoblast markers is observed, this would suggest that these are not the targets of p53. The qRT-PCR from Experiment II uses a broad array of markers that are linked to diverse cellular processes including cell-cycle regulation, apoptosis, senescence and DNA repair function (Levine, 1997). Therefore, any significant up-regulation in p53 markers can be followed up for further study

6 Conclusion

It is possible that an increase in p53 levels and subsequent repression of Osx is one of the underlying mechanisms that cause the MS phenotype due to DHODH mutations. If the hypothesis is accepted, then the next approach should be to determine the pathways by which p53 is activated (such as increased cellular stress due to mitochondrial dysfunction), and the

additional downstream mechanisms that contribute to the MS phenotype, in combination with p53-dependent repression of Osx. Conversely, if the results show that p53 is not involved in MS, then the mouse model itself can be used for future analysis, thus providing avenues for further research.

7 Acknowledgements

I wish to thank Dr. Paul Tranior, and A/Prof Daisuke Sakai for providing guidance on this project with regards to my hypothesis, and A/Prof Irfaan Saadi and Dr Joe Rainger for advising me on the appropriate experimental protocols, and referring me to the appropriate online tools. Also, I wish to thank Leonard Zon, Frank Wagener, and Richard Whiter for responding to my emails about their studies and providing me with additional papers to help me consolidate my ideas.

8 Appendices

A Supplementary Data

The data provided in the table below summarises the mutations and their effects. Data is sourced from Ng et al. (2010), Rainger et al. (2012),and Fang et al. (2012)

Table 3: Summary of *DHODH* Human mutations

Mutation	Exon	Amino acid change	Effect of mutation	Localisation	Enzyme activity (%)
56G>A	2	G19E	No data	No data	68.2
155A>G	2	E52G	No data	No data	7.3
403C>T	3	R135C	Impairment in substrates binding activity	Proper Mitochondrial localisation	56.9
454G>A	4	G152R	No data	No data	13.5
605G>C	5	G202D	No data	No data	55.8
595C>T	5	R199C	No data	No data	47.6
611T	5	L204PfsX8	No data	No data	0
605G>A	5	G202A	Reduced protein stability	Proper Mitochondrial localisation	6.0
730C>T	6	R244W	No data	No data	66.7
851C>T	7	T284I	No data	No data	56.6
1036C>T	8	R346W	Reduced protein stability	Proper Mitochondrial localisation	45.3
1022C>T	8	R326X	No data	No data	No data
1069G>A	8	A357T	No data	No data	No data
1175A>G	9	D392G	No data	No data	53.8

B Appended papers

European Journal of Oral Sciences

Eur J Oral Sci 2016; 124: 241–245
DOI: 10.1111/eos.12270

European Journal of Oral Sciences

Dihydroorotate dehydrogenase depletion hampers mitochondrial function and osteogenic differentiation in osteoblasts

JingXian Fang[1,2,3,4,*], Haruyoshi Yamaza[1,*], Takeshi Uchiumi[2], Yoshihiro Hoshino[1], Keiji Masuda[1], Yuta Hirofuji[1], Frank A. D. T. G. Wagener[3], Dongchon Kang[2], Kazuaki Nonaka[1]

[1]Department of Pediatric Dentistry, Graduate School of Dental Science, Kyushu University, Fukuoka, Japan; [2]Department of Clinical Chemistry and Laboratory Medicine, Graduate School of Medical Sciences, Kyushu University, Fukuoka, Japan; [3]Department of Orthodontics and Craniofacial Biology, Radboud Institute for Molecular Life Sciences, Radboud University Medical Centre, Nijmegen, the Netherlands; [4]Department of Pediatric Dentistry, Guangdong Provincial Stomatological Hospital, Southern Medical University, Guangzhou, China

*These authors contributed equally to this work.

Fang J, Yamaza H, Uchiumi T, Hoshino Y, Masuda K, Hirofuji Y, Wagener FADTG, Kang D, Nonaka K. Dihydroorotate dehydrogenase depletion hampers mitochondrial function and osteogenic differentiation in osteoblasts.
Eur J Oral Sci 2016; 124: 241–245. © 2016 Eur J Oral Sci

Mutation of the dihydroorotate dehydrogenase (*DHODH*) gene is responsible for Miller syndrome, which is characterized by craniofacial malformations with limb abnormalities. We previously demonstrated that DHODH was involved in forming a mitochondrial supercomplex and that mutated *DHODH* led to protein instability, loss of enzyme activity, and increased levels of reactive oxygen species in HeLa cells. To explore the etiology of Miller syndrome in more detail, we investigated the effects of DHODH inhibition in the cells involved in skeletal structure. Dihydroorotate dehydrogenase in MC3T3-E1 cells derived from mouse calvaria osteoblast precursor cells was knocked down by specific small interfering RNAs (siRNAs), and cell proliferation, ATP production, and expression of bone-related genes were investigated in these cells. After depletion of DHODH using specific siRNAs, inhibition of cell proliferation and cell cycle arrest occurred in MC3T3-E1 cells. In addition, ATP production was reduced in whole cells, especially in mitochondria. Furthermore, the levels of runt-related transcription factor 2 (*Runx2*) and osteocalcin (*Ocn*) mRNAs were lower in DHODH siRNA-treated cells compared with controls. These data suggest that depletion of DHODH affects the differentiation and maturation of osteoblasts. This study shows that mitochondrial dysfunction by DHODH depletion in osteoblasts can be directly linked to the abnormal bone formation in Miller syndrome.

Haruyoshi Yamaza, Department of Pediatric Dentistry, Graduate School of Dental Science, Kyushu University, 3-1-1 Maidashi, Higashi-ku, Fukuoka 812-8582, Japan

E-mail: hyamaza@dent.kyushu-u.ac.jp

Key words: MC3T3-E1 cells; Miller syndrome; mitochondria; osteogenesis

Accepted for publication February 2016

Miller syndrome is a rare genetic condition referred to as 'postaxial acrofacial dysostosis' and its clinical symptoms consist of blossom front, hypoplasia, cleft lip and/or palate, and depletion of the fifth digits (1, 2). Dihydroorotate dehydrogenase (*DHODH*) was recently identified, by a whole-exome sequencing strategy, as the causative gene for Miller syndrome, and 11 different *DHODH* mutations have been found in patients with Miller syndrome (3).

Dihydroorotate dehydrogenase gene contains nine exons encoding a 43-kDa protein with an N-terminal mitochondrial-targeting signal, a transmembrane domain, and a large catalytic domain (3). Dihydroorotate dehydrogenase catalyses the fourth enzymatic step of the de novo pyrimidine biosynthetic pathway by converting dihydroorotate into orotate and is localized on the outer surface of the inner membrane of mitochondria. The other enzymes involved in de novo pyrimidine biosynthesis are localized in the cytoplasm (4, 5).

Mitochondria produce ATP and regulate biological processes such as cell signaling, cell death, cell growth and differentiation, and multiple metabolic pathways (5, 6). Using HeLa cells, we previously demonstrated that DHODH interacted with mitochondrial respiratory chain complexes II and III, and its mutation might, in part, affect the pathogenesis of Miller syndrome through altered mitochondrial function (7). In addition, we showed that Miller syndrome-based mutations of DHODH led to protein instability as well as to loss of DHODH activity. Depletion of DHODH in HeLa cells affects mitochondrial function, as exemplified by reduced membrane potential, increased production of reactive oxygen species, and instability of the electron transfer chain (8).

However, it remains unknown how mitochondrial dysfunction by DHODH depletion leads to abnormal development of the pharyngeal arches and causes Miller syndrome. As many of the clinical craniofacial symptoms in Miller syndrome are related to bone formation, we used the osteoblast precursor cells, MC3T3-E1 cells, and investigated the function of DHODH in these cells using its specific small interfering RNAs (siRNAs). It was shown that disruption of DHODH affected the mitochondrial function and bone formation in the cells, and we postulated that dysfunction of DHODH in the osteoblasts might be linked to the symptoms of Miller syndrome.

Material and methods

Antibodies and chemicals

Antibody against DHODH was raised in our laboratory. Antibody against β-actin was purchased from Sigma (St Louis, MO, USA). Antibodies against cyclinB1 and p53 were purchased from Santa Cruz (Santa Cruz, CA, USA). Antibodies against cyclin-dependent protein kinase Cdk1/Cdc2 (CDC2) and phosphorylated retinoblastoma (phospho-RB) were purchased from Cell Signaling (Beverly, MA, USA).

Cell culture

Mouse calvaria-derived osteoblast precursor cells, MC3T3-E1 cells, were kindly provided by Dr Fukuda. MC3T3-E1 cells were cultured in alpha-Minimal Essential Medium (αMEM) containing 10% heat-inactivated FBS and 1% penicillin/streptomycin in an atmosphere of 5% CO_2 at 37°C. Subconfluent cell cultures were subcultured using trypsin/EDTA (Gibco, Carlsbad, CA, USA) and plated in 24-well multiwell plates containing αMEM/10% FBS, at 1×10^4 cells well^{-1}.

Knockdown analysis using siRNAs

The following two different types of 25-bp double-stranded DHODH siRNA generated from Stealth Select RNAi (Invitrogen, Carlsbad, CA, USA) were used: 5′-AUUUAUGGCCCAGAACUCUCACUUC-3′ and 5′-GAAGUGAGAGUUCUGGGCCAUAAAU-3′ as DHODH si#1; and 5′-AUACCUGUUAAUGACAGCUUGGUCC-3′ and 5′-GGACCAAGCUGUCAUUAACAGGUAU-3′ as DHODH si#2. Transfection of siRNA was performed using oligofectamine (Invitrogen), according to the manufacturer's instructions. Briefly, 2.5 μl of oligofectamine was diluted in 100 μl of Opti-MEM medium (Invitrogen) and incubated for 5 min at room temperature. Twenty-five picomoles of DHODH siRNA or control duplex Stealth RNAi (Invitrogen) was added and mixed gently to Opti-MEM containing oligofectamine, and incubated for 20 min at room temperature. Oligomer–oligofectamine complexes were combined with aliquots of 1×10^4 MC3T3-E1 cells in 2 ml of serum-free culture medium and incubated for 5 min at room temperature. The cells were seeded in 6-well multiwell plates with 2 ml of culture medium and cultured in an atmosphere of 5% CO_2 at 37°C.

Cell proliferation assay

To determine cell proliferation, MC3T3-E1 cells transfected with control or each DHODH siRNA were seeded in triplicate in 24-well multiwell plates, at a density of 1×10^4 cells per well, and cultured in αMEM with dialysed 10% FBS (Invitrogen). Cells were trypsinized and counted daily, for up to 72 h, using a Coulter Counter (Beckman Coulter, Fullerton, CA, USA).

Western blotting

MC3T3-E1 cells were lysed in TNE lysis buffer (50 mM Tris/HCl, pH 7.5, 1 mM EDTA, 150 mM NaCl, and 0.5% Nonidet P-40). Twenty micrograms of protein was separated by SDS-PAGE and immunoblotted with the indicated specific antibodies. The signals were visualized

Table 1
List of primers for RT-PCR

Target gene	Forward primer sequence (5′–3′)	Reverse primer sequence (5′–3′)	Annealing temperature (°C)	Cycle number	Product size (bp)	GenBank accession no.
Runx2	CCGCACGACAACCGCACCAT	CGCTCCGGCCCACAAATCTC	58	28	289	XM_006523548.1
Ocn	AAGCAGGAGAGGGCAATAAGGT	AGCTGCTGTGACATCCATAC	65	30	292	NM_001037939.2
Gapdh	CACCATGGAGAAGGCCGGGG	GACGGACACATTGGGGGTAG	60	28	418	XM_001476707.2

Gapdh, glyceraldehyde-3-phosphate dehydrogenase; *Ocn*, osteocalcin; *Runx2*, runt-related transcription factor 2.

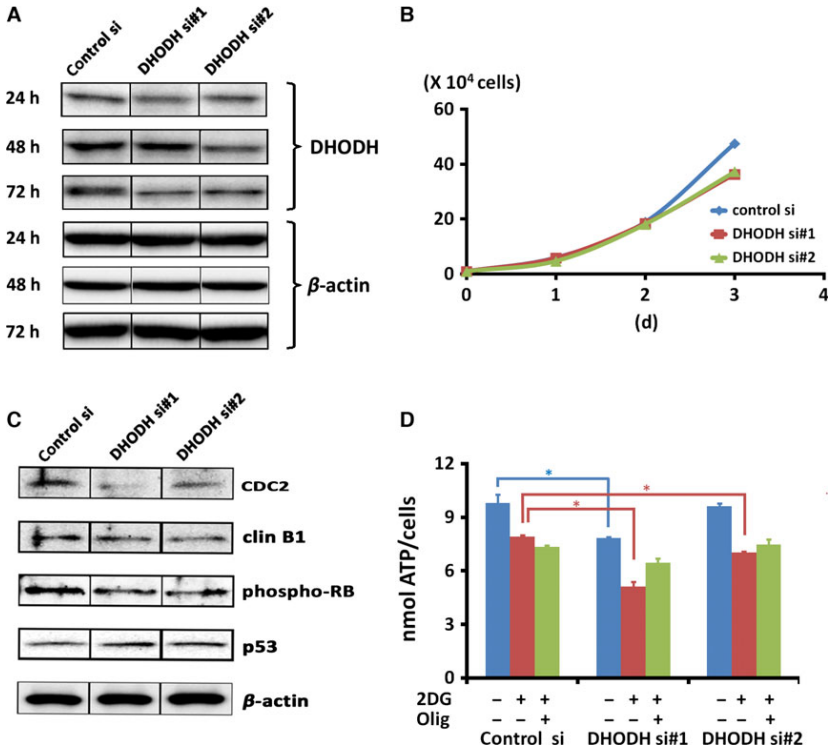

Fig. 1. Effects of small interfering RNA (siRNA)-mediated dihydroorotate dehydrogenase (DHODH) knockdown. (A) Two different siRNAs for DHODH (DHODH si#1 and DHODH si#2) were transfected into MC3T3-E1 cells. The levels of DHODH in MTC3T3-E1 cells were analysed 24, 48, and 72 h after treatment with siRNA. Beta-actin is shown, at each time point, as an internal control. (B) Proliferation of siRNA-transfected MC3T3-E1 cells. At the time points indicated, the cells were harvested and counted using a cell counter. Cell proliferation was reduced by depletion of DHODH (i.e. by treatment with DHODH si#1 and DHODH si#2). The data represent mean ± SE ($n = 3$). (C) Analysis of cell cycle-related proteins in MC3TC-E1 cells treated with DHODH siRNAs. The cells were lysed 72 h after treatment with DHODH siRNA and immunoblotted with antibodies against cyclin-dependent protein kinase Cdk1/Cdc2 (CDC2), cyclin B1 (clin B1), phosphorylated retinoblastoma (phospho-RB), p53, and β-actin (the internal control). (D) ATP production was decreased in MC3TC-E1 cells treated with DHODH siRNAs. ATP production was decreased by reduction of DHODH in whole cells (lane 1) and mitochondria (lane 2). Each bar and line represent mean + SE ($n = 3$). *$P < 0.05$ vs. control. 2DG, 2-deoxy-D-glucose, Olig, oligomycin.

with horseradish peroxidase (HRP)-labelled anti-rabbit IgG and an enhanced chemiluminescence reagent (GE Healthcare, Cleveland, OH, USA). The chemiluminescence was recorded and quantified usig a chilled charge-coupled device camera (LAS1000plus; Fuji Photo Film, Tokyo, Japan) and its attached software (Image Reader LAS-1000 Lite; Fuji Photo Film).

ATP quantification

Cellular ATP was quantified using an ATP-determination kit, according to the manufacturer's instructions (Promega, Madison, WI, USA). Briefly, cells were lysed in passive lysis buffer (Promega) and equal volumes of cell lysate were added to the standard reaction solution. The luminescence was measured and normalized to the amount of protein in each lysate. The values were determined in the linear range of the assay using a standard curve.

RNA extraction and RT-PCR analysis

After 72 h of treatment with DHODH siRNA, MC3T3-E1 cells were lysed using Trizol reagent (Invitrogen) and total RNA was extracted as described in the manufacturer's protocol. Total RNA was treated with RNase-free DNase I (Promega) and purified using an RNeasy kit (Qiagen, Mainz, Germany). cDNA was synthesized with 1 μg of total RNA using ReverTraAce (Toyobo, Osaka, Japan). PCR amplifications for mouse runt-related transcription factor 2 (*Runx2*), Osteocalcin (*Ocn*) and glyceraldehyde-3-phosphate dehydrogenase (*Gapdh*) were performed using QuickTaq (Invitrogen) and the PCR products were subjected to electrophoresis on a 2% agarose gel. The gel was stained with ethidium bromide, and gene expression levels were quantified using NIH image (http://rsb.info.nih.gov/nih-image/). Sequences for mouse-specific primers and the PCR condition for each gene are shown in Table 1.

Statistical analysis

Statistical comparisons between groups were analysed using the Student's *t*-test or, where appropriate, the paired *t*-test. Significance was determined at $P < 0.05$.

Results

To elucidate the molecular mechanisms of Miller syndrome, we analyzed the function of DHODH in osteo-

blast precursor cells, using DHODH siRNA. The level of DHODH protein was reduced in MC3T3-E1 cells by two different types of DHODH siRNAs after 72 h of treatment, whereas the expression of β-actin was not affected by treatment with DHODH siRNA (Fig. 1A). A nontargeting siRNA (control siRNA) confirmed the specificity of the DHODH siRNAs and did not affect the expression of DHODH and β-actin (Fig. 1A).

Knockdown of DHODH inhibits cell proliferation

To investigate the effects of DHODH depletion on cell proliferation, we closely examined the cell growth rate following the knockdown of DHODH. The number of viable MC3T3-E1 cells during each treatment with siRNA was counted using a Coulter Counter (Beckman Coulter) and it was observed that cell proliferation was decreased in DHODH siRNA-treated cells compared with control siRNA-treated cells (Fig. 1B).

Effects of knockdown of DHODH on the cell cycle

Similar inhibition of cell growth was found earlier in HeLa cells after inhibition of DHODH and was accompanied by cell cycle arrest at the G2/M phase (7). To investigate the cause of the reduced proliferation of MC3T3-E1 cells in more detail, the expression of several proteins involved in the cell cycle was analysed. Compared with HeLa cells, the expression of CDC2, cyclinB1, and phospho-RB was slightly decreased in MC3T3-E1 cells after knockdown of DHODH, whereas expression of p53 was slightly increased (Fig. 1C). These results demonstrate that G1/S arrest may occur in MC3T3-E1 cells treated with DHODH siRNAs.

Knockdown of DHODH reduces cellular and mitochondrial ATP production

Energy production is one of the functions of mitochondria and is important in cell growth (5). Dihydroorotate dehydrogenase is the only enzyme localized in mitochondria among the enzymes involved in de novo pyrimidine synthesis (9). To investigate involvement of DHODH in mitochondrial function during bone formation, we measured cellular ATP levels in MC3T3-E1 cells treated with control and DHODH siRNAs. After treatment with siRNA, all DHODH siRNA groups showed a lower ATP base level, especially the group treated with DHODH si#1 (Fig. 1D).

To analyse specifically mitochondrial ATP production, we used 2-deoxy-D-glucose (2DG), an analogue of glucose that blocks the first step of the glycolysis pathway. The production of ATP from the mitochondria was significantly decreased in MC3T3-E1 cells treated with both DHODH si#1 and si#2 siRNAs, compared with the control siRNA (Fig. 1D). Furthermore, co-incubation with oligomycin, an inhibitor of complex V in the respiratory chain of the mitochondria, strongly reduced the mitochondrial production of ATP in all groups (Fig. 1D). Therefore, these results show that depletion of DHODH leads to mitochondrial dysfunction in osteoblast precursor cells, which complements our previous work on Miller syndrome using HeLa cells (7).

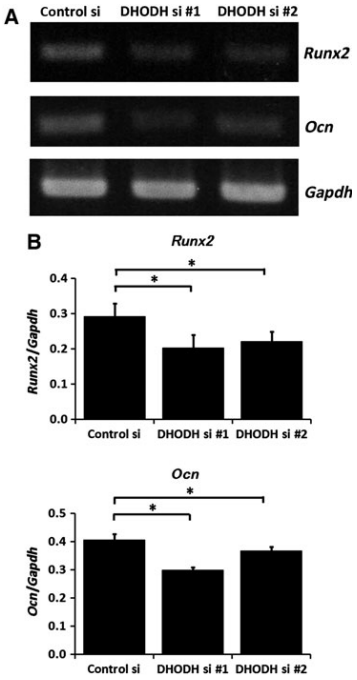

Fig. 2. Analysis of expression of the osteogenic genes, runt-related transcription factor 2 (*Runx2*) and osteocalcin (*Ocn*), in MC3T3-E1 cells by treatment with dihydroorotate dehydrogenase (DHODH) small interfering RNA (siRNA). (A) Representative images of agarose gels are shown. (B) Quantification of gene expression is shown in the bar chart. As an internal control, glyceraldehyde-3-phosphate dehydrogenase (*Gapdh*) is used and the expression of each gene is calculated quantitatively by normalization to the expression of *Gapdh*. Each bar and line represent the mean + SE ($n = 3$). *$P < 0.05$ vs. control.

Osteogenic gene expression

Bone formation depends on the proliferation and differentiation of osteoblasts and is required for skeletal development. Osteoblast differentiation requires the initial commitment of mesenchymal stem cells, followed by induction of tissue-specific patterns of gene expression (10). Runt-related transcription factor 2 is a transcriptional factor essential for osteoblast differentiation (11). Osteocalcin is secreted from osteoblasts and is involved in promotion of bone formation (12). After knockdown of DHODH in MC3T3-E1 cells, the levels of expression of both *Runx2* and *Ocn* genes were significantly decreased (Fig. 2). These results show that reduction of DHODH interferes with normal bone formation.

Discussion

In this study, we demonstrated that DHODH reduction in osteoblast precursor cells induced: (i) retardation of cell growth with G1/S arrest; (ii) decreased ATP pro-

duction by mitochondria; and (iii) reduction of osteogenic gene expression. Miller syndrome is inherited in an autosomal-recessive or compound heterozygous manner (3). It is recognized that DHODH mutations are found (3) and the development of the first and second pharyngeal arches is disrupted (1, 2) in patients with Miller syndrome. Therefore, Miller syndrome is related to abnormal skeletal structures and is caused by DHODH dysfunction. Previously, we investigated DHODH function in mitochondria using HeLa cells, which were derived from human cervical carcinoma (7, 8). In HeLa cells, we observed that DHODH depletion induced mitochondrial dysfunction and cell cycle arrest, and proposed that impairment of DHODH activity was linked to mitochondrial dysfunction, causing the Miller syndrome phenotype. Although we analysed DHODH function in cancer cells, the molecular mechanisms of DHODH in cells involved in the skeletal structure are not yet completely understood.

We, therefore, used osteoblast precursor cells to elucidate the function of DHODH in these cells in greater detail and to explore the aetiology of Miller syndrome. In MC3T3-E1 cells, which were derived from mouse calvaria osteoblast precursor cells, cell proliferation was reduced by treatment with DHODH siRNA, and ATP production in MC3T3-E1 cells was decreased in whole cells, especially in mitochondria during treatment with DHODH siRNA (Figs 1B,C). Previously, we reported that DHODH was physically associated with the respiratory chain complexes II and III, and mitochondrial dysfunction was observed by DHODH knockdown in HeLa cells (7). Therefore, DHODH may be associated with respiratory chain complexes II and III in MC3T3-E1 cells, and reduction of DHODH would lead to decreased ATP production through mitochondrial dysfunction, causing reduced cell proliferation.

RUNX2 is a transcription factor and *Runx2* is a master gene necessary for differentiation of mesenchymal stem cells into osteoblasts (11). Osteocalcin is secreted from osteoblasts and is involved in promoting bone formation (12). These genes are thus important during the differentiation and maturation of osteoblasts. In MC3T3-E1 cells with reduced levels of DHODH, the levels expressed of these osteogenic genes were significantly decreased (Fig. 2). Our results suggest that osteoblast maturation is arrested by mitochondrial dysfunction through DHODH reduction, which may be linked to the abnormal bone formation in Miller syndrome.

In conclusion, we demonstrated that depletion of DHODH affected cell proliferation and osteogenic gene expression in osteoblasts through mitochondrial dysfunction, suggesting that DHODH could be involved in the differentiation and maturation of osteoblasts. Therefore, dysfunction of osteoblasts by DHODH reduction might be linked to the clinical symptoms of Miller syndrome.

Patients with Miller syndrome have a variety of other clinical symptoms, as well as craniofacial dysostosis. Therefore, in the future, DHODH function should be investigated in various tissues and cells, including neural crest cells, to elucidate, in further detail, the molecular mechanisms involved in Miller syndrome.

Acknowledgements – We thank Dr Takao Fukuda, Department of Periodontology, Faculty of Dental Science, Kyushu University for providing us with MC3T3-E1 cells. This study was supported, in part, by Grants-in-aid for Scientific Research (C) (No. 25463187 to H.Y.), Young Scientific Research (B) (No. 23792433 to H.Y.), and Challenging Exploratory Research Project (No. 23659967 to K.N.) from the Japan Society for Promotion of Science.

References

1. Donnai D, Hughes HE, Winter RM. Postaxial acrofacial dysostosis (Miller) syndrome. *J Med Genet* 1987; **24**: 422–425.
2. Miller M, Fineman R, Smith DW. Postaxial acrofacial dysostosis syndrome. *J Pediatr* 1979; **95**: 970–975.
3. Ng SB, Buckingham KJ, Lee C, Bigham AW, Tabor HKK, Dent M, Huff CD, Shannon PT, Jabs EW, Nickerson DA, Shendure J, Bamshad MJ. Exome sequencing identifies the cause of a mendelian disorder. *Nat Genet* 2010; **42**: 30–35.
4. Evans DR, Guy HI. Mammalian pyrimidine biosynthesis: fresh insights into an ancient pathway. *J Biol Chem* 2004; **279**: 33035–33038.
5. McBride HM, Neuspiel M, Wasiak S. Mitochondria: more than just a powerhouse. *Curr Biol* 2006; **16**: R551–R560.
6. De Michele R, Carimi F, Frommer WB. Mitochondrial biosensors. *Int J Biochem Cell Biol* 2014; **48**: 39–44.
7. Fang J, Uchiumi T, Yagi M, Matsumoto S, Amamoto R, Takazaki S, Yamaza H, Nonaka K, Kang D. Dihydro-orotate dehydrogenase is physically associated with the respiratory complex and its loss leads to mitochondrial dysfunction. *Biosci Rep* 2013; **33**: e00021.
8. Fang J, Uchiumi T, Yagi M, Matsumoto S, Amamoto R, Saito T, Takazaki S, Kanki T, Yamaza H, Nonaka K, Kang D. Protein instability and functional defects caused by mutations of dihydro-orotate dehydrogenase in Miller syndrome patients. *Biosci Rep* 2012; **32**: 631–639.
9. Rawls J, Knecht W, Diekert K, Lill R, Loffler M. Requirements for the mitochondrial import and localization of dihydroorotate dehydrogenase. *Eur J Biochem* 2000; **267**: 2079–2087.
10. Franceschi RT. The developmental control of osteoblast-specific gene expression: role of specific transcription factors and the extracellular matrix environment. *Crit Rev Oral Biol Med* 1999; **10**: 40–57.
11. Komori T, Yagi H, Nomura S, Yamaguchi A, Sasaki K, Deguchi K, Shimizu Y, Bronson RT, Gao YH, Inada M, Sato M, Okamoto R, Kitamura T, Yoshiki S, Kishimoto T. Targeted disruption of Cbfa1 results in a complete lack of bone formation owing to maturational arrest of osteoblasts. *Cell* 1997; **89**: 755–764.
12. Hosoda K, Kanzaki S, Eguch H, Kiyoki M, Yamaji T, Koshihara Y, Shiraki M, Seino Y. Secretion of osteocalcin and its propeptide from human osteoblastic cells: dissociation of the secretory patterns of osteocalcin and its propeptide. *J Bone Miner Res* 1993; **8**: 553–565.

Cell Death and Differentiation (2017) 24, 2022–2031
 1350-9047/17

www.nature.com/cdd

p53 inhibits SP7/Osterix activity in the transcriptional program of osteoblast differentiation

Natalia Artigas[1], Beatriz Gámez[1], Mónica Cubillos-Rojas[1], Cristina Sánchez-de Diego[1], José Antonio Valer[1], Gabriel Pons[1], José Luis Rosa[1] and Francesc Ventura*[,1]

Osteoblast differentiation is achieved by activating a transcriptional network in which *Dlx5*, *Runx2* and *Osx/SP7* have fundamental roles. The tumour suppressor p53 exerts a repressive effect on bone development and remodelling through an unknown mechanism that inhibits the osteoblast differentiation programme. Here we report a physical and functional interaction between *Osx* and *p53* gene products. Physical interaction was found between overexpressed proteins and involved a region adjacent to the OSX zinc fingers and the DNA-binding domain of p53. This interaction results in a p53-mediated repression of OSX transcriptional activity leading to a downregulation of the osteogenic programme. Moreover, we show that p53 is also able to repress key osteoblastic genes in *Runx2*-deficient osteoblasts. The ability of p53 to suppress osteogenesis is independent of its DNA recognition ability but requires a native conformation of p53, as a conformational missense mutant failed to inhibit OSX. Our data further demonstrates that p53 inhibits OSX binding to their responsive Sp1/GC-rich sites in the promoters of their osteogenic target genes, such as *IBSP* or *COL1A1*. Moreover, p53 interaction to OSX sequesters OSX from binding to DLX5. This competition blocks the ability of OSX to act as a cofactor of DLX5 to activate homeodomain-containing promoters. Altogether, our data support a model wherein p53 represses OSX–DNA binding and DLX5–OSX interaction, and thereby deregulates the osteogenic transcriptional network. This mechanism might have relevant roles in bone pathologies associated to osteosarcomas and ageing.
Cell Death and Differentiation (2017) **24,** 2022–2031; doi:10.1038/cdd.2017.113; published online 4 August 2017

Osteoblast differentiation is triggered by a variety of intra- and extracellular osteogenic signals, such as BMPs, IGFs and Wnts.[1] The process commences with a mesenchymal stem cell (MSC) precursor becoming an osteochondroprogenitor cell, which is later sequentially transformed into a mature osteoblast.

It is also well known that osteochondroprogenitor maturation and the subsequent conversion of pre-osteoblasts to mature osteoblasts is controlled by a network of specific transcription factors. Among these, *Runx2* and *Osterix/SP7* (*Osx)* have a critical role in osteogenesis.[2,3] *Runx2* deletion in mice causes a severe impairment in the development of the skeleton and *Runx2* mutations in humans are causative of cleidocranial dysplasia disorder.[4] Similarly, *Osx* deletion impairs the consecution of a mature osteoblast phenotype and was proven to be important in the maintenance of bone homeostasis, because its postnatal deletion causes loss of bone mass and bone defects.[5,6] Several studies also found that *SP7/Osx* mutations or SNPs are related to osteoporosis and *osteogenesis imperfecta*.[7,8] For these reasons, *Osx* and *Runx2* are mandatory for the development of the skeleton. Moreover, both cooperatively regulate the expression of key genes in bone biology forming a transcriptional complex.[9] OSX also acts as a necessary cofactor for DLX family of transcription factors.[10] Furthermore, these transcription factors are subjected to fine tuning by posttranscriptional regulation. For instance, MAP kinases phosphorylate DLX5, RUNX2 and OSX, leading to their activation.[11–13] These studies highlighted the complexity of the transcription factor network, which controls the osteoblast differentiation process and bone development.

Maturation of MSCs to the osteoblastic phenotype is a multistep process that requires cell expansion, differentiation and survival. The tumour suppressor p53 is considered a master regulator of proliferation and apoptosis. p53 activity helps to eliminate damaged cells, preventing tumorigenesis.[14] Furthermore, p53 has been linked to cell differentiation in a variety of cell types, such as neurons, muscular cells and osteoblasts.[15–17] Surprisingly, despite the key cellular functions of p53, *Trp53* knockout mice did not show major developmental defects. However, detailed studies demonstrated skeletal abnormalities in some animals, such as upper incisor fusion and craniofacial and limb malformations.[18] *Trp53* knockout mice are also characterized by a denser skeleton than their wild-type littermates and the *Trp53*-deficient bone marrow-derived MSCs (BM-MSCs) have a higher capacity to differentiate towards the osteoblastic fate.[17,19] The impact of p53 on the osteoblastic transcription factor network is also evident, as cells with the *Trp53* deletion overexpress *Osx* and osteogenic genes through an unknown mechanism.[17]

Previous studies suggested that *p53* deletion allows overactivation of the BMP pathway by mechanisms that involve changes in the expression of *Smad1* or *Smurf1*.[20,21] It has also been shown that p53 and RUNX2 proteins interact, blocking Runx2 transcriptional activity, and that p53 regulates *Runx2*

[1]Departament de Ciències Fisiològiques, Universitat de Barcelona, IDIBELL, L'Hospitalet de Llobregat, Spain

*Corresponding author: Francesc Ventura, Departament de Ciències Fisiològiques, Universitat de Barcelona, IDIBELL, C/Feixa Llarga s/n, E-08907 L'Hospitalet de Llobregat, Spain. Tel: +34 934024281; Fax: +34 934024268; E-mail: fventura@ub.edu

Received 23.9.16; revised 21.4.17; accepted 12.6.17; Edited by S Fulda; published online 04.8.17

expression levels by an miRNA-mediated mechanism.[22,23] Therefore, although the inhibitory role of p53 in bone formation is well established, little is yet known about the molecular mechanisms by which p53 exerts this function. Moreover, an in-depth understanding of the role of p53 in bone biology could have implications in the knowledge of pathologies associated with p53 signalling network alterations.

Our work focused in the identification of the molecular mechanisms by which p53 exerts a repressive effect over the osteoblast differentiation programme. We found, using either loss- or gain-of-function models, that p53 expression has a negative impact on the expression of osteoblast-specific transcription factors and their targets. Our work further demonstrated that the negative role of p53 is independent of p53 transcriptional activity but instead required physical interaction between OSX and p53 at the protein level. p53 prevented OSX from binding to Sp1/GC-rich sequences and blocked OSX from interacting with DLX5 and binding to homeodomain sequences.

Results

p53 downregulates osteoblastic gene expression. It has been previously established that p53 has an inhibitory role in osteoblast differentiation using mouse models.[17,24] There is also evidences suggesting that these phenotypes are cell autonomous, as the BM-MSCs from *p53*-deficient mice show enhanced differentiation *in vitro*.[19] To further characterize the molecular mechanism underlying these phenotypes, we first evaluated osteoblastic gene expression from primary osteoblasts obtained from *Trp53* knockout or wild-type mice. Absence of p53 results in upregulation of important genes implicated in bone development (Figure 1a). Importantly, two transcription factors with relevant roles in bone biology, *Dlx5* and *Osx*,[11,25] were 2-fold and 3.5-fold overexpressed, respectively. Furthermore, *Runx2* showed a slight upregulation at the mRNA level. OSX target genes were also upregulated in *Trp53* knockout osteoblasts, such as *Ibsp* (bone sialoprotein) or *Bglap* (osteocalcin).[9,26,27]

To confirm these results, we used the p53-inducible SaOs2 cell line SaOs2-p53TetOn, which only expresses p53 upon the addition of doxycycline (Figure 1b). Treatment with doxycycline for 24 h confirmed the p53-dependent inhibition of O*SX*, *DLX5*, *IBSP* and *COL1A1* expression. The upregulation of *BGLAP* expression after induction of p53 expression could be explained by direct binding of p53 to the known p53-responsive sequences in *BGLAP* promoter.[28,29] These results provide evidence of a p53-dependent downregulation of the expression of osteoblastic genes.

As previous studies had identified the involvement of the osteogenic BMP pathway on p53's effects, we next focused on this signalling pathway and its modulation by p53. As previously reported, p53 deletion results in a slight upregulation of *Smad1* mRNA, as well as the BMP-target gene *Id1* in primary osteoblasts [16,30] (Supplementary Figure 1A, left panel). Interestingly, an induction of *Smad7* was found in p53 knockout osteoblast. In accordance a 1.4-fold upregulation of *SMAD7* expression was obtained after induction of p53

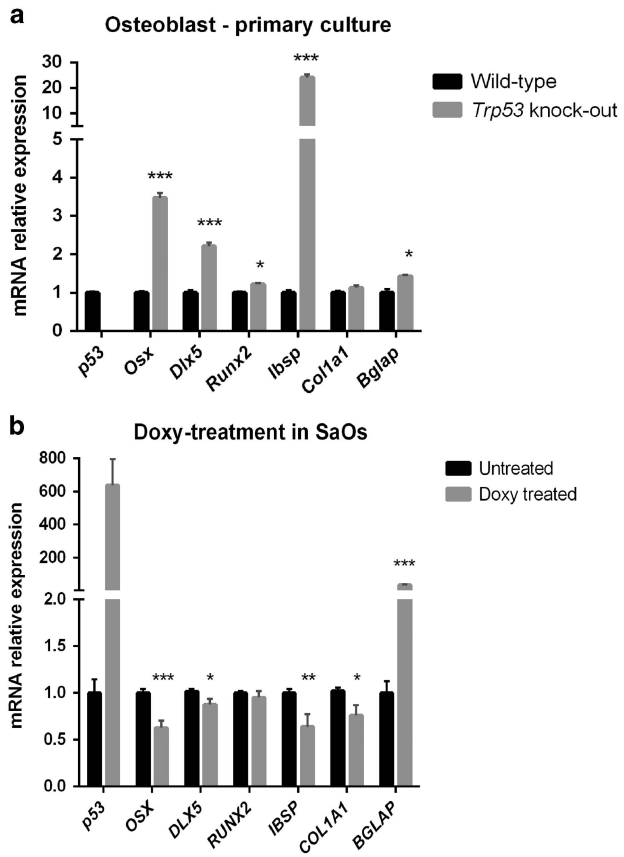

Figure 1 p53 protein inhibits osteogenic differentiation transcriptional programme. (**a**) mRNA expression levels of primary osteoblasts from wild-type or *Trp53* knockout mice grown for 3 days in osteogenic differentiation medium, and (**b**) SaOs2-p53TetOn were treated for 24 h with doxycycline 2 nM in 1% FBS medium. *Bglap* indicates *Osteocalcin* gene mRNA. mRNAs were measured by RT-qPCR, normalized to *TBP* and expressed as relative expression ± S.E.M. of at least three independent experiments (*$P<0.05$, **$P<0.01$, ***$P<0.001$, using the Student's *t*-test)

in SaOs2 cells, but no substantial changes in the expression of *SMAD1* or *ID1* (Supplementary Figure 1A, right panel).

SaOs2-p53TetOn cells were also incubated with doxycycline for 16 h and treated with 2 nM BMP2 for 2 h. Our results failed to detect significant differences in pSMAD1/5/8 levels in either primary osteoblasts or the SaOs2-p53TetOn model (Supplementary Figures 1B and C). Moreover, expression of genes such as *JUNB*, *SMAD7* or *DLX5*, which are direct targets of Smad-transcription factors, was independent of p53 induction and only *ID1* displayed a minor downregulation in the doxycycline-treated condition (Supplementary Figure 1D). Thus, these minor negative effects of p53 on the BMP pathway likely could not explain the changes observed in osteogenic gene expression.

p53 physically interacts with Osx. In order to identify the mechanisms involved in inhibition of osteogenic gene expression by p53 we focused on two drivers of bone development, RUNX2 and OSX. As a mechanism by which p53 inhibits RUNX2 through physical interaction has been described previously in a DNA-damage context,[22] we also tested the capacity of p53 to bind to RUNX2 and OSX. To

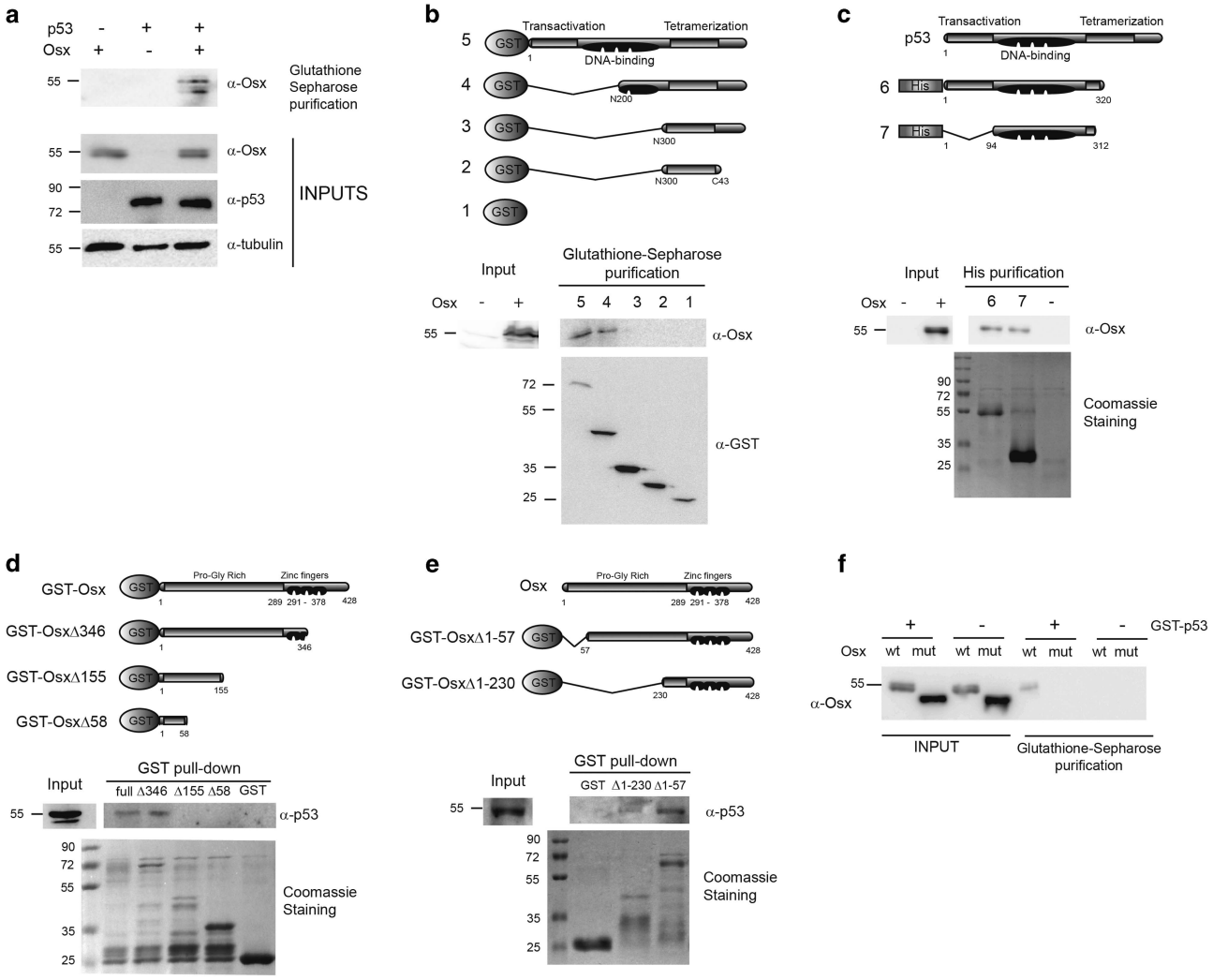

Figure 2 p53 protein physically interacts with OSX. (**a**) SaOs2 cells were infected with retroviral expression vectors for human Osx and/or GST-tagged human p53. Extracts from cells and Glutathione-Sepharose co-precipitated proteins were visualised by immunoblotting using anti-p53 and anti-Osx antibodies. (**b**) Extracts from HEK293T cells transfected with *Osx* expression vector in combination with the indicated GST-p53-chimeric protein were incubated with Glutathione-Sepharose beads for 1 h. Co-precipitated proteins were identified by immunoblotting using anti-OSX antibody. (**c**–**e**) Cell extracts were incubated with the indicated chimeric protein bound to Glutathione-Sepharose (**d** and **e**) or Ni^{2+} (**c**) beads overnight. Interacting proteins were identified by immunoblotting using anti-p53 or anti-OSX antibodies. (**f**) Lysates from HEK293T cells expressing murine wild-type *Osx* or the double mutant S73A/S77A in combination with the p53-chimeric protein or GST were incubated with Glutathione-Sepharose beads. Interacting proteins were identified by immunoblotting using anti-OSX antibody

assess this, we retrovirally infected SaOs2 cells with OSX and GST-tagged p53 expression vectors. OSX co-purified with p53, suggesting that they interact in osteogenic cells (Figure 2a). To map the involved interaction sites, we expressed *Osx* in combination with different truncated GST-p53 expression vectors in mammalian cells. OSX was able to bind to the N-terminal region of p53 protein in intact cells (Figure 2b). We further pinpoint the p53 domain involved in such interaction by studying OSX binding to recombinant N-terminal truncated p53 (Figure 2c). Altogether, the data demonstrate that the p53 DNA-binding domain is sufficient for physical interaction with OSX. We also verified which domain of OSX was involved in the interaction. Our results showed that p53 requires a region that encompasses part of the transactivation domain proximal to the OSX zinc fingers (Figures 2d and e). We also determined whether the activation status of OSX influences its interaction with p53. A less active form of OSX (the OSX S73A/S77A mutant, which cannot be phosphorylated by MAP kinases) showed lower interaction with p53 in intact cells (Figure 2f).

Similar assays with GST-p53 expression vectors showed that RUNX2 was able to bind to the N-terminal domain of p53 in mammalian cells (Supplementary Figure 2A). Recombinant truncated RUNX2 proteins showed that RUNX2 requires the PST region to physically interact with p53 (Supplementary Figure 2B).

Osx transcriptional activity is inhibited by interaction with p53. We next assessed the effect of p53 interaction on OSX transcriptional activity. We evaluated the expression

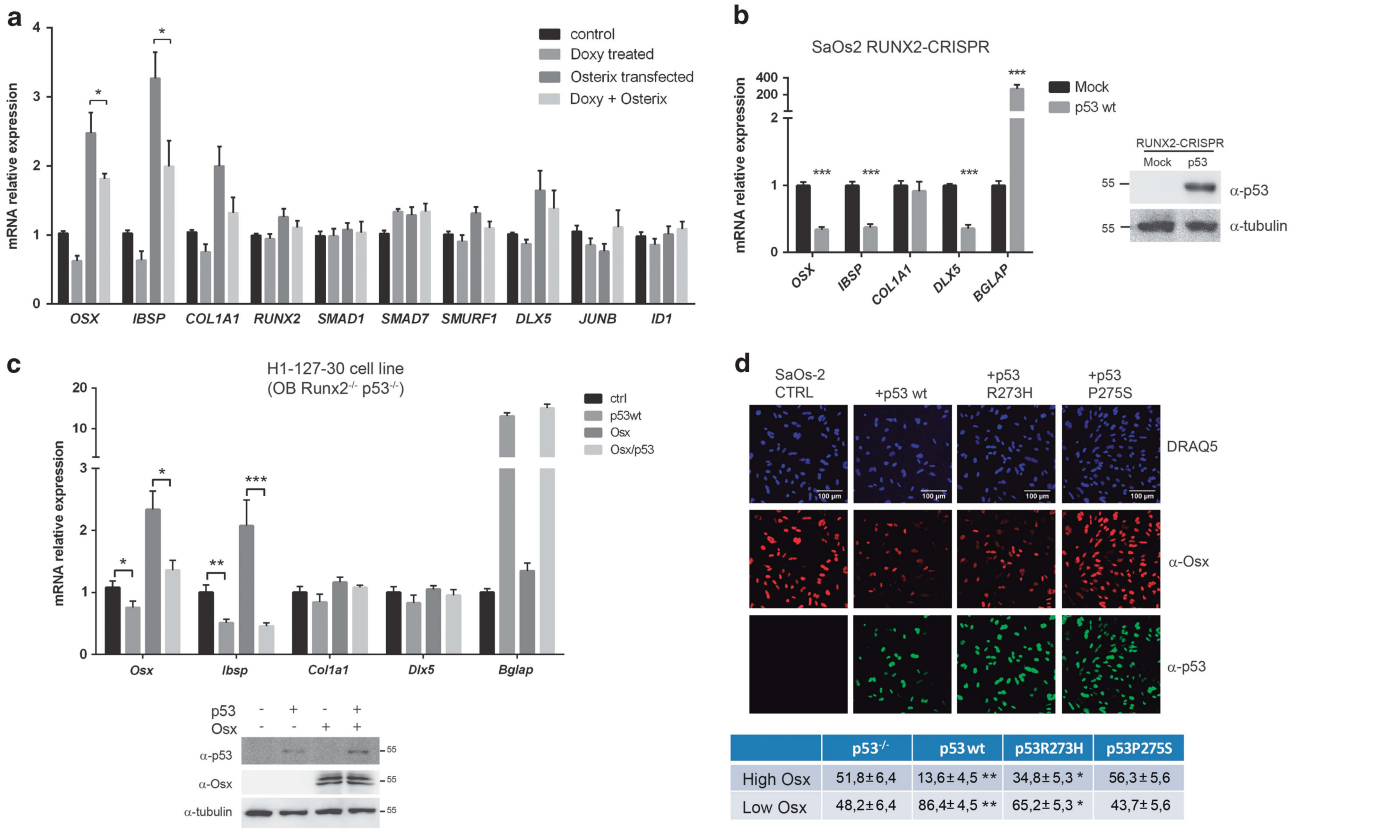

	p53-/-	p53 wt	p53R273H	p53P275S
High Osx	51,8± 6,4	13,6± 4,5 **	34,8± 5,3 *	56,3± 5,6
Low Osx	48,2± 6,4	86,4± 4,5 **	65,2± 5,3 *	43,7± 5,6

Figure 3 p53 regulates osteoblastic gene expression inhibiting OSX transcriptional activity. (**a**) mRNA expression levels in SaOs2-p53TetOn treated for 24 h with 2 nM doxycycline and/or transfected with *Osx* expression vector. mRNA was measured by qRT-PCR, normalized to *TBP* and expressed as relative expression ± S.E.M. of at least three independent experiments. (**b**) mRNA expression levels in SaOs2 *RUNX2*-CRISPR cells retrovirally infected with murine p53 expression vector. Right panel shows a western blotting to verify p53 expression. (**c**) H1-127-30 osteoblasts generated from the double *Runx2* and *Trp53* knockout mice were infected with retroviral expression vectors for murine p53 and OSX. mRNAs were measured by RT-qPCR, normalized to *TBP* and expressed as relative expression ± S.E.M. from six independent experiments. (**d**) Immunocytofluorescence of SaOs2 cells infected with retroviral expression vectors carrying murine p53 wild type, human p53R273H and murine p53P275S. Immunostaining was performed with anti-OSX and anti-p53 antibodies and nuclei visualized using DRAQ5. Quantification of OSX relative expression levels (cut-off point at <150 OSX intensity) are expressed as percentage of cells. Statistics were performed against the p53 knockout condition. (*$P<0.05$, **$P<0.01$, ***$P<0.001$ using the Student's *t*-test)

of genes implicated in the osteoblastic differentiation programme on SaOs2-p53TetOn cells overexpressing OSX in combination with doxycycline treatment (Figure 3a). Both controls and cells overexpressing OSX had a lower induction of OSX target genes (such as *OSX* itself and *IBSP*[27,31]) when p53 was expressed. The qPCR assay only detected endogenous *OSX* expression; thus, these data provide additional evidence of OSX regulation of its own promoter.[31] These observations suggest that OSX transcriptional activity is inhibited by p53.

p53 has been shown to repress RUNX2 function.[23] For this reason, we then analyzed whether the effects of p53 on osteogenic gene expression were derived from inhibition of RUNX2 or also depended on the inhibition of OSX transcriptional activity. Two distinct approaches were performed: first, generation of pools of SaOs2 cells, which are p53-deficient, where the third exon of the *RUNX2* gene was inactivated by CRISPR technology (Supplementary Figure 3A). Second, analysis of the osteoblast cell line H1-127-30 generated from the double *Runx2*/*p53* knockout mice.[32] The *RUNX2*-specific CRISPR deletion was confirmed by immunoblot, obtaining a pool of cells with 60% reduction of RUNX2 levels (Supplementary Figure 3B). Expression of p53 in these cells still conferred a strong downregulation of osteogenic genes (Figure 3b). Similarly, re-expression of p53 in *Runx2*$^{-/-}$ *p53*$^{-/-}$ osteoblasts led to inhibition of *Osx* and *Ibsp* expression, and abolished their induction by ectopic OSX (Figure 3c). Altogether, these data suggest that the inhibitory effects of p53 on osteogenic gene expression depend not only on RUNX2 but also on OSX inhibition.

We also analyzed by immunofluorescence whether p53 could block OSX trafficking to the nucleus. First, we visualized that OSX expression in SaOs2-p53TetOn cells was localized in the nucleus regardless of p53 expression. Second, at the single-cell level the expression of p53 was negatively correlated with that of OSX (Supplementary Figure 4). To further confirm the negative correlation between p53 and OSX protein levels, we infected p53-deficient SaOs2 cells with retrovirus expressing murine wild-type p53, the human contact mutant p53R273H or the murine structural mutant p53P275S. Whereas the p53R273H changes the Arg273 involved in base recognition, p53P275S (corresponding to P278S in the human p53 gene) alters the structure of the its DNA-binding domain.[33–35] Expression of wild-type p53 or the p53R273H

mutant induced a strong downregulation of endogenous OSX expression, whereas the p53P275S mutant did not significantly changed OSX levels (Figure 3d).

Osx–DNA binding is blocked by p53 protein. A mechanism by which p53 could inhibit OSX transcriptional activity could be affecting its affinity for DNA. We evaluated the OSX ability to bind to Sp1/GC-rich sequences (which have been shown to be OSX responsive elements[12,26] by performing an oligo-pull-down assay using a sequence of the bone enhancer from the *Col1a1* promoter.[26] We expressed OSX in *Trp53* knockout osteoblasts using retrovirus and tested the affinity of OSX for the oligonucleotide. Co-infection with a murine wild-type p53 retrovirus led to a 60–70% lower OSX binding affinity for the Sp1/GC-rich sites (Figure 4a). We also co-infected the p53-deficient osteoblasts with the transcriptionally inactive human p53R273H mutant. Co-expression of this mutant also reduced OSX binding to the oligonucleotide, which refutes the possibility of a p53-dependent transcriptional mechanism underlying OSX binding inhibition (Figure 4a). These results *in vitro* were confirmed by chromatin immunoprecipitation (ChIP) in SaOs2, where expression of wild-type p53 reduced OSX and RUNX2 occupancy in the responsive regions of the promoter of their target genes *IBSP*, *COL1A1* and *BGLAP* (Figure 4b). Expression of the human p53R273H mutant also reduced recruitment of OSX to *IBSP*, *COL1A1* and *BGLAP* promoters, whereas OSX binding was not significantly reduced by p53P275S (Figure 4b).

In accordance with it, the expression levels of the OSX target genes were repressed by the presence of murine wild-type p53 and the human p53R273H contact mutant in *Trp53* knockout osteoblast (Figure 4c). However, p53P275S failed to induce repression of these genes. To verify the mechanism that confers differential inhibition of OSX activity by distinct p53 mutants, we analyzed the physical interaction of OSX with wild-type p53, and the R273H and P275S mutants. Purification of OSX from extracts of SaOs2 cells retrovirally expressing *Osx* and *p53* mutants demonstrate that physical interaction between OSX and p53P275S was reduced compared with the interaction with wild type and R273H mutant (Figure 4d). These results confirm that the effects on OSX transcriptional activity are not dependent on p53 transcriptional activity, but on protein-protein interaction. Together, these data suggest regulation of OSX transcriptional activity by p53 at protein level via blockage of the OSX interaction with their Sp1/GC-rich responsive sites.

The OSX interaction network is inhibited by p53. It has recently been described that OSX acts as a cofactor for the DLX transcription factor family.[10] As p53 binds close to the OSX zinc-finger domain implicated in the OSX–DLX5 interaction, we investigated the impact of p53 binding on the OSX–DLX5 complex. First, we analyzed whether p53 could disrupt the OSX–DLX5 complex. We performed GST-DLX5 pull-down assays using extracts from SaOs2-p53TetOn cells infected with murine wild-type p53 or the human R273H mutant. As previously described OSX bound DLX5,[10] but both wild type p53 and the R273H mutant disrupted this interaction (Figure 5a). Thus, p53 could likely inhibit OSX transcriptional activity in promoters regulated by the OSX–DLX complex.

As mentioned before, OSX is able to regulate its own promoter[31] and our group had also previously identified DLX5 as an activator of the proximal promoter of *Osx*.[11] The *Osx* promoter $-114/-51$ contains a Sp1/GC-rich box that could be a target for direct OSX binding, as well as a DLX5-binding homeobox. Luciferase assays using this *Osx* promoter region showed that both OSX and DLX5 activated the *Osx* promoter, and they showed an additive effect when expressed together (Figure 5b). More importantly, activation of the *Osx* promoter was repressed by p53. Mutation of either the homeobox or the Sp1/GC-rich sequences reduced the ability of DLX5 and OSX to activate transcription from the *Osx* promoter, suggesting that both sites are relevant for their function. To further discern whether the inhibition of p53 on the *Osx* promoter is through inhibition of OSX binding to the GC-rich box or instead by avoiding its role as a DLX5 cofactor, we performed an oligo-pull-down assay using the $-114/-51$ *Osx* promoter. We tested the capacity of OSX and DLX5 to bind to the wild-type $-114/-51$ sequence (pOsx HB-wt), or to the sequence with the homeobox site mutated (pOsx HB-mut) (Figure 5c). Assays from doxycycline-treated SaOs2-p53TetOn cells confirmed that OSX was able to bind to this promoter region probably using the Sp1/GC-rich box, besides binding to the homeobox, given that OSX was still able to bind to the HB-mut oligonucleotide. As expected, DLX5 bound to the HB-wt and showed lower affinity to the HB-mut oligonucleotide. The presence of p53 not only reduced OSX binding to both sequences but also blocked the binding of DLX5 to the homeobox site. These results were confirmed by chromatin-immunoprecipitation in SaOs2-p53TetOn cells, where induction of p53 strongly reduced DLX5 occupancy in the *Osx* promoter (Figure 5d). Therefore, binding of both DLX5 and OSX to their sites were inhibited by p53. Altogether, our results suggest a novel mechanism of OSX regulation, as summarized in Figure 6. p53 inhibits OSX transcriptional and osteogenic activity by binding close to its zinc-finger region, repressing its interaction with DNA and its transcriptional partners, such as DLX5.

Discussion

Cell differentiation and proliferation are usually thought of as antagonistic events in many cell types, with differentiation being only possible after blockage of proliferation. As a canonical tumour suppressor, p53 is supposed to inhibit proliferation but also promote differentiation.[36] However, the inhibitory role of p53 in osteogenic differentiation, in a cell-autonomous manner, is well established by mouse genetics and cell-based approaches.[19] Although the p53-null mouse shows enhanced bone mineral density, Mdm2-conditional knockout results in a severe impairment of bone formation.[17,24] Interestingly, MSCs derived from induced pluripotent stem cells from Li–Fraumeni patients carrying the transcriptionally inactive p53G245D mutation showed deficient osteoblast differentiation. Moreover, deletion of p53 in these iPS cells eliminated the osteogenic differentiation defect suggesting that osteogenic effects are derived from gain-of-function activities of mutant p53.[37]

Despite this evidence, the exact nature of the mechanisms that underlie these p53 effects remained unknown. Our work identifies these effects on osteoblast differentiation through repression of OSX activity by direct interaction with p53. Previous studies focused on the impact of the p53 family over osteogenic BMP signalling with interesting findings such as

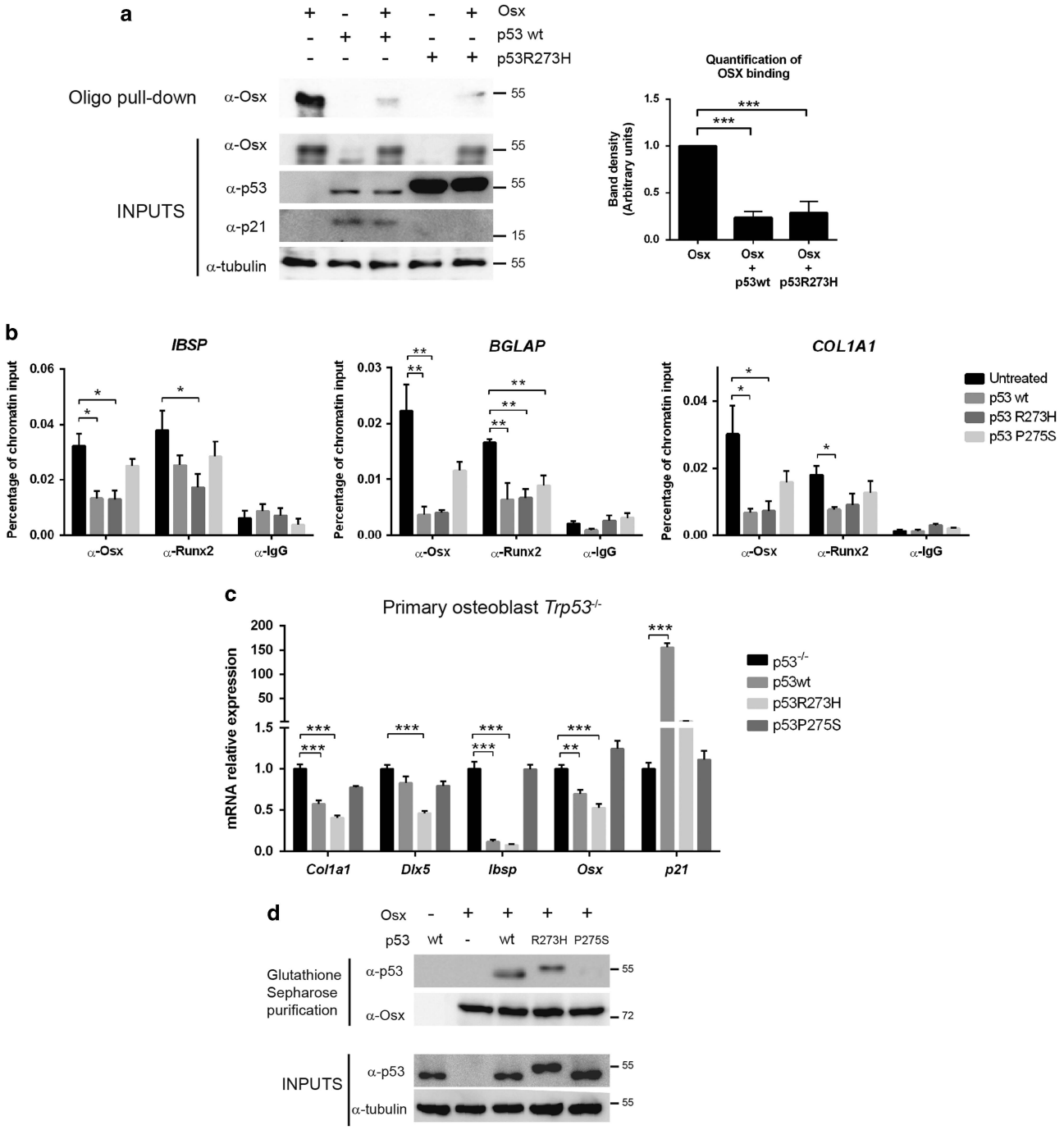

Figure 4 p53 blocks OSX binding to Sp1 elements. (**a**) Oligo-pull-down assay was performed using a biotinylated-oligonucleotide containing the *Col1a1* bone-enhancer sequence. The oligonucleotide was incubated with extracts from *Trp53* knockout primary osteoblasts retrovirally infected with the indicated expression vectors. Bar graph on the right shows the quantification of the OSX band after streptavidin-purification relative to their input levels. (**b**) ChIP from SaOs2 cells infected with retroviral expression vectors for murine p53 wild-type, human p53R273H and murine p53P275S. DNA–protein complexes were isolated with antibodies against Osx, Runx2 and IgG. Specific primers for the promoters of *IBSP*, *BGLAP* (Osteocalcin) and *COL1A1* bone-enhancer were used for qRT-PCR analysis. Results are represented relative to input chromatin. (**c**) *Trp53* knockout primary osteoblasts were retrovirally infected with murine p53 wild-type or p53P275S or human p53R273H mutant forms. *p21* gene was used as reporter of p53 transcriptional activity. mRNA was measured by qRT-PCR, normalized to *Tbp* and expressed as relative expression ± S.E.M. of at least three independent experiments (*$P<0.05$, **$P<0.01$, ***$P<0.001$, using Student's *t*-test). (**d**) SaOs2 cells were infected with retrovirus expression vectors for murine GST-tagged Osx and p53 wild-type and P275S from mouse or human p53R273H. Extracts from SaOs2 cells and Glutathione-Sepharose co-precipitated proteins were visualised by immunoblotting using anti-p53 and anti-Osx antibodies

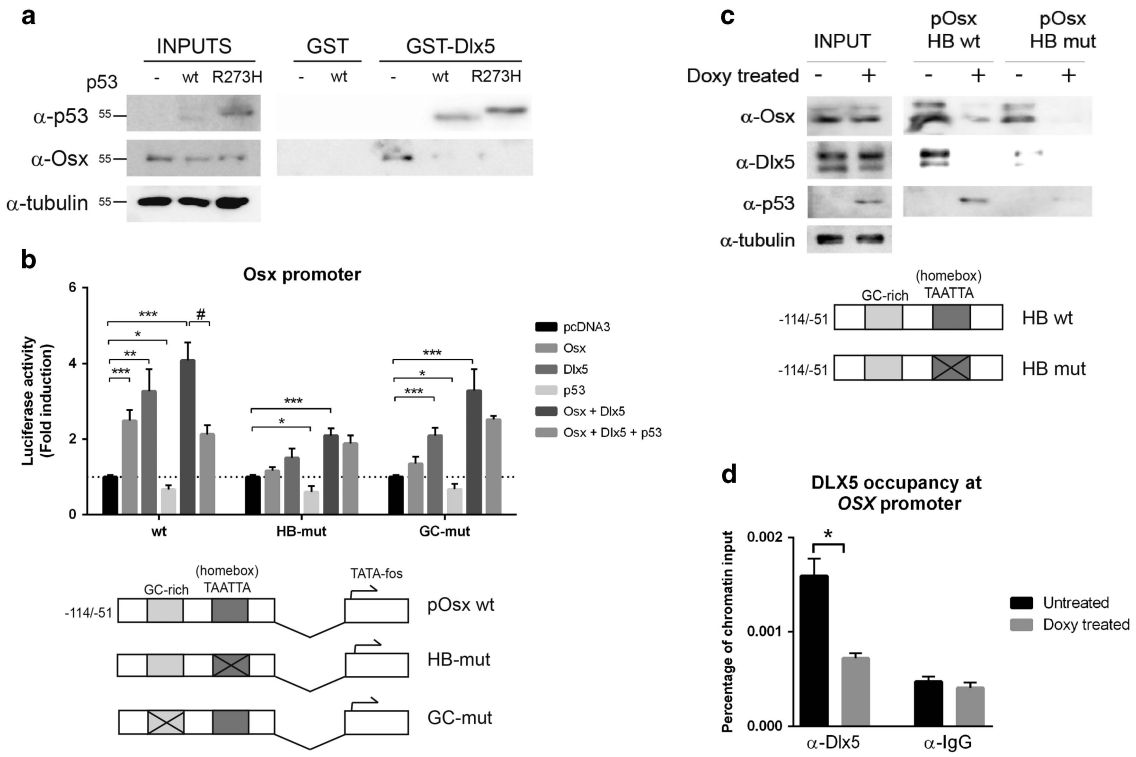

Figure 5 Inhibition of *Osx* promoter is mediated by p53 blocking DLX5-OSXx complex. (**a**) Extracts of SaOs2-p53TetOn retrovirally infected with the indicated p53-expression vectors were incubated with the indicated chimeric protein bound to Glutathione-Sepharose beads overnight. Interacting proteins were identified by immunoblotting using anti-Osx and anti-p53 antibodies. (**b**) SaOs2 cells were co-transfected with the indicated expression vectors, or empty pcDNA3 vector as control, and the murine −114/−51 Osterix-promoter luciferase reporter, wild-type or with the indicated mutated versions. HB-mut is the reporter with the homeodomain box mutated; GC-mut indicates mutation in the Sp1/GC-rich box.[11] Scheme of the −114/−51 Osterix-promoter is shown. Luciferase activity was measured and normalized against *β*-galactosidase activity, and represented as fold induction compared with the pcDNA3 transfection condition. # is used to compare Osx+Dlx5 *versus* Osx+Dlx5+p53 conditions. (**c**) Oligo-pull down using biotinylated −114/−51 Osterix-promoter sequence (pOsx HB wt) and its homeobox-mutated version (pOsx HB mut). Extracts from SaOs2-p53TetOn untreated or treated for 24 h with 2 nM doxycycline were used. Interacting proteins were identified by immunoblotting using anti-OSX, anti-DLX5 and anti-p53. (**d**) SaOs2-p53TetOn were treated or not with 2 nM doxycycline for 24 h. DNA-protein complexes were isolated with antibodies against DLX5 and IgG. Specific primers for the *Osx* promoter were used for qRT-PCR analysis. Results are represented relative to input chromatin from three independent experiments (*$P<0.05$)

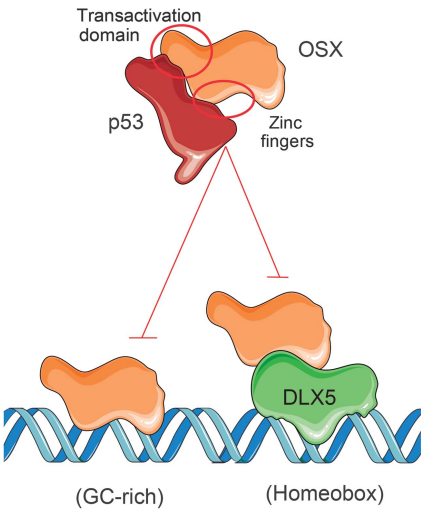

Figure 6 Schematic representation of the proposed p53-OSX network: p53 blocks Osterix transcriptional activity by physical interaction. We suggest that p53-OSX interaction prevents OSX from binding to Sp1/GC-rich sequences, and also interferes in the formation of the OSX–DLX5 transcriptional complex, that responds to homeobox sequences

the p53-Smad1/5 physical interaction,[38] or Smad1 upregulation due to the lack of p53.[16,20] Our data suggest that these changes were of low magnitude. We also identified positive regulation of the gene expression of the Smad signalling inhibitor *Smad7*. These data are in agreement with data from epithelial cells, which establishes that p53 family members bind to the *Smad7* promoter through a p53-response element.[39]

As mentioned above, our work and previous studies revealed that p53 represses the expression of osteoblast-determining transcription factors independently of p53–DNA binding.[17,37] Our data further demonstrated the ability of p53 to inhibit the transcriptional osteogenic programme independent of p53–DNA binding on the basis of several lines of evidence. First, a transcriptionally inactive mutant form of human p53 (R273H) similarly blocked OSX function, whereas a murine conformational mutant (P275S) had lower inhibitory ability. Second, RUNX2-deficient osteoblasts were also sensitive to the inhibitory effects of p53. Third, p53 was able to repress binding to DNA and cooperative transcriptional effects of endogenous and ectopic OSX and DLX5.

Osx, *Runx2* and *Dlx5* are mandatory transcriptional regulators of the osteogenic process. Their gene products

physically interact and lead to a strong cooperation in the transcription of target genes and the production of a mineralized bone matrix.[9,10] Previous studies also depict an integrative feed-forward transcriptional network involving *Runx2*, *Osx* and *Dlx5*, in which they positively regulate each other´s transcription.[9,11,40–43] These fully integrated relationships suggest that any alteration in the function of any of them would result in a de-regulation of the whole network. Thus, the p53-mediated inhibition of OSX function could be an important factor in the maintenance of bone homeostasis under physiological conditions. p53 signalling mutations, which lead to high p53 protein expression levels,[44,45] would disturb the function of the *Dlx5-Runx-Osx* network with important consequences.

The DNA-binding domain of p53 interacts with an OSX domain adjacent to its zinc fingers. Similarly, we also mapped the PST transactivation domain of RUNX2 as its p53-interaction region. Interaction between p53 and OSX results in downregulation of *Osx* target genes involved in bone matrix maturation, such as *Ibsp*, *Col1a1* and *Osx* itself. The *Osx* proximal promoter, the first known molecular target of p53 inhibition,[17] is positively controlled through direct DNA binding by OSX and DLX5 proteins.[11,27,31] We determined that p53 interaction does not alter OSX localization but impairs OSX–DNA binding *in vitro* and *in vivo* to their canonical Sp1/GC-rich sites. Moreover, p53 also inhibits OSX–DLX5 transcriptional complex formation and binding to homeobox sequences. Importantly, the OSX–DLX5 complex co-occupy most the bone enhancer regions in genome-wide analysis and evolutionary analysis showed correlation with the evolution of skeletal formation.[10] As p53 and DLX5 share the region of interaction with OSX,[10] it is plausible to infer that higher levels of p53 would abrogate OSX–DLX5 complex formation. By blocking these two DNA-binding mechanisms of action of OSX, p53 breaks two important mechanisms of the osteoblast transcriptional programme.

Our findings that p53 has a transcriptionally independent role in OSX function suggest important physiopathological consequences. Proliferation and differentiation should co-exist in a coordinated manner to maintain tissue homeostasis over time. Besides its major role in the transcriptional control of proliferation and apoptosis, p53 might block osteogenic differentiation from mesenchymal precursors to allow its expansion and prevent their shortage from premature specification. Deregulation of these networks would lead to osteoporosis by shortage of mesenchymal precursors and/or misdirected differentiation towards alternative fates such as adipocytes, which are both characteristic features of ageing.[46] Several reports indicate that loss of osteogenic potential and increased adipogenesis of bone progenitors during senescence is dependent on p53 and correlated with lower *Osx* expression.[47] Moreover, the shift from osteoblastogenesis to increased adiposity observed in osteopenias induced by ageing, accelerated senescence or ovariectomy correlated with upregulation of p53 levels.[46]

The relation between p53 mutations and osteosarcomagenesis has been highlighted in several studies.[36,48,49] Osteosarcoma is largely composed of poorly differentiated cells[50] and the p53 loss-of-function is enough for the development of osteosarcoma.[51] Previous studies, aimed at detecting the origin of the osteosarcoma, point to dedifferentiated osteoblastic cells, rather than MSCs.[36,37,49,50] In addition, most p53 mutations are missense and impair DNA binding, but give rise to the gain of new oncogenic functions.[52,53] Our data suggest a possible negative correlation between p53 and OSX protein levels that varies depending on p53 specific mutation (Figure 3d). Therefore, the definition of p53 status and its mutation in osteosarcomas likely could help us to understand its effect on osteogenic differentiation, and to better tackle the progression of the disease. Altogether, our data support a model where p53 represses OSX–DNA binding and OSX–DLX5 interaction and thereby deregulates the osteogenic transcriptional network.

Materials and Methods

Mouse model. *Trp53* knockout mice B6.129S2-*Trp53*tm1Tyj/J from Jackson Laboratories (Bar Harbor, ME, USA) were kindly provided by Dr J Martin-Caballero. Mice were housed under controlled conditions (12 h light/12 h dark cycle, 21 °C, 55% humidity) and fed *ad libitum* with water and a 14% protein diet (Teklad 2014, Harlan, Santa Perpètua de Mogoda, Barcelona, Spain). All animal experiments were performed in accordance with guidelines approved by the Ethical Committee for Animal Experimentation of the University of Barcelona and Generalitat de Catalunya (Spain).

Cell culture. SaOs2-p53TetOn, kindly provided by Dr R Bartrons, and HEK293T (American Type Culture Collection, Rockville, MD, USA) cell lines were maintained in DMEM supplemented with 10% fetal bovine serum (FBS), 2 mM glutamine, 1 mM pyruvate, 100 U/ml penicillin and 0.1 mg/ml streptomycin. The isolation of primary osteoblasts from calvaria was carried out as described previously.[54] Primary osteoblasts and H1-127-30 osteoblast cell line [32] were maintained in α-MEM supplemented with 10% FBS, 2 mM glutamine, 1 mM pyruvate, 100 U/ml penicillin and 0.1 mg/ml streptomycin. As osteogenic differentiation medium, osteoblast medium was supplemented with 50 μM ascorbic acid and 10 mM β-glycerophosphate. HEK293T cells were transiently transfected using polyethylenimine, and SaOs2 using Lipofectamine-LTX (Invitrogene). Retroviral infection in *Trp53* knockout osteoblasts, H1-127-30 and SaOs2 cells were performed as described previously.[55] Doxycycline treatment (2 nM) was carried out in media with 1% FBS. BMP2 (R&D, Minneapolis, MN, USA) was used at 2 nM.

CRISPR-Cas9. The *RUNX2* gene was knocked down in SaOs2 cells using the system described by Ran *et al.*[56]. The gRNA sequence was designed to target the exon 3 of the *RUNX2* gene. The guide sequence was cloned into the pSpCas9(BB)-2A-Puro vector donated by R. Estevez and confirmed by sequencing. The primers used were: F:5′CACCGGCTGGTGCTCGGATCTACGG3′ and R:5′-AAACCCG TAGATCCGAGCACCAGCC-3′. SaOs2 cells were plated in six wells and transfected overnight. An empty vector without gRNA was used as negative control. Puromycin was added at 1 μg/ml and maintained three days for selection. The selected cells were tested for *RUNX2* gene deletion by endonuclease assay. The following primers were used for *RUNX2* amplification: F:5′-CAAACTTGATTTCTCACCTCCTCA-3′ and R:5′-TTCAAGGTAAGAGGCTACACCGC-3′. The positive pools were expanded and checked for RUNX2 knock-down by immunoblot.

Plasmids and reagents. Murine Osterix expression vectors were kindly provided by Dr B de Crombrugghe. The Osx S73A/S77A, GST-Osx, GST-OsxΔ346 and GST-OsxΔ155 GST-Dlx5 were previously described,[9,12] and GST-OsxΔ58, GST-OsxΔ1–57 and GST-OsxΔ1–230 were generated by double digestion from GST-Osx. GST-Runx2 and GST-Runx2Δ230 were kindly provided by Dr M Montecino. The GST-p53 and their derivatives were kindly provided by Dr Y Xiong. The human His-p53-(1–320) and His-p53-(94–312) were a gift from Dr Arrowsmith (Addgene plasmid 24864 and 24866, respectively). The pMXs-p53 and pMXs-p53P275S from mouse were a gift from Dr Yamanaka (Addgene plasmids 22725 and 22726, respectively).[57] The pMXs-p53R273H was generated from pLenti6/V5-p53_R273H (from Dr Futscher, Addgene plasmid 22934)[58] by subcloning the human p53R272H sequence into pMXs plasmid. Human pMXs-Osx was a gift from Dr O Mazda. The pBABE-GST-p53 retroviral expression vector

was generated from pEBG-GST-p53. The pBABE-GST-OSX was generated from pGEX-Osx.

Pull-down assays. For *in vitro* GST-pull down experiments, the assays were performed as described previously.[9] For analysis of the physical interaction assays in mammalian cells, the GST-p53 or the GST-Osx vectors were co-transfected with *Osx* or the distinct p53 mutant expression vectors in HEK293T or retrovirally infected in SaOs2 cells and cells were lysed after 48 h. Lysates were collected, centrifuged to eliminate debris and purified by binding to Glutathione-Sepharose beads for 1 h at 4 °C. Then, the beads were washed with washing buffer (50 mM Tris/HCl, 150 mM NaCl, 0.1% Igepal-CA630 plus protease and phosphatase inhibitors) three times. Bound proteins were detected by immunoblotting. For *in vitro* pull down of His-tagged proteins, all used buffers were supplemented with 10 mM imidazol and bound to Ni^{2+} resin for purification.

Luciferase assay. SaOs2 cells were cultured in 24-well plates and transfected for 8 h with Lipofectamine LTX with the indicated plasmids. Transfection efficiency was assessed by GFP expression. Luciferase activities were quantified 48 h post-transfection using the Luciferase assay system (Promega, Madison, WI, USA) and normalized using the β-Galactosidase Detection Kit II (Clontech, Mountain View, CA, USA).

Oligo-pull-down assays. Oligo-pull-down assays were carried out as previously described.[26] The pOsx HB-wt and pOsx HB-mut oligonucleotides were generated by PCR using biotinylated primers from the proximal Osterix murine promoter, and wild-type or homeobox-mutated $-114/-51$ *Osterix* promoter sequences as templates. The Sp1 oligonucleotide sequence was generated from the *Col1a1* promoter as previously described.[26]

Western blot assay. Identification of proteins, from cell extracts or pull-down assays, was performed by immunoblotting against phospho-Smad1/5/8, Smad1 (Cell Signaling 9743 and 13820, Danvers, MA, USA), Osx (Abcam 22552, Cambridge, UK), Runx2 (MBL D130-3, Woburn, MA, USA), p53 (Cell Signaling 48818), Id1 (C-20 sc-488) and p21 (C-19 sc-397) (Santa Cruz Biotechnology, Dallas, TX, USA) or α-tubulin (Sigma-Aldrich T5168, St. Louis, MO, USA), diluted at 1 : 1000. Antibodies against Dlx5 (C-20 sc-18152 and Y-20 sc-18151) (Santa Cruz Biotechnology) were used at 1 : 500. Immunoreactive bands were detected with horseradish-peroxidase-conjugated secondary antibodies and an ECL-kit (Biological Industries, Cromwell, CT, USA).

ChIP assay. ChIP assay was carried out as described in Artigas *et al.*[9]. $SaOs_2$ p53TetOn cells were cultured until confluence before overnight doxycycline treatment. $SaOs_2$ were retrovirally infected with the distinct p53 mutant constructs. ChIP was carried out using 1 μg of the indicated antibodies: anti-Osx (Abcam), anti-Runx2 (MBL), anti-Dlx5 (C-20 sc-18152 and Y-20 sc-18151, 0.5 μg each) or anti-IgG (Upstate) as a control, and purified with 20 μl Magna ChIP Protein A+G Magnetic Beads (Millipore, Billerica, MA, USA). The DNA fragments were purified using the QIAquick Gel Extraction Kit (Qiagen, Hilden, Germany) and analyzed by qRT-PCR. The primers used for the qRT-PCR analysis for *IBSP* and *COL1A1* were previously described.[9] *BGLAP* primers were R: 5′-CCGTAGGCCAAACCCCAG AGGATATGT-3′ and F: 5′-CTCTGCTTGAACCTATTTTAGGTCTCTGA-3′. *OSX* primers were: R: 5′-CCTGCTTCCCACCCCTTCCA-3′ and F: 5′-ATGAGGAGG GCGAGAGAGGG-3′.

Immunocytofluorescence. SaOs2 p53TetOn immunofluorescence was performed as previously described[9] using 1 : 100 p53 (Cell Signaling) and 1:250 anti-Osterix (Abcam).

qRT-PCR analysis. Total RNA was isolated from primary osteoblasts or SaOs2 cells using TRIsure reagent (Bioline, London, UK). Purified RNA was reverse-transcribed using the High-Capacity cDNA Reverse Transcription Kit (Applied Biosystems, Foster City, CA, USA). Quantitative PCRs were carried out using the ABI Prism 7900 HT Fast Real-Time PCR System and Taqman 5′-nuclease probes (Applied Biosystems). Designed Taqman assays (Applied Biosystems) were used to quantify gene expression. All transcripts were normalized to *Tbp* expression.

Statistical analysis. Statistical analysis was performed using the Student's *t*-test. Quantitative data are presented as means $\pm$ S.E.M. Differences were considered significant at $^{*}P<0.05$, $^{**}P<0.01$ and $^{***}P<0.001$.

Conflict of Interest

The authors declare no conflict of interest.

Acknowledgements. We thank Drs B de Crombrugghe, J Martín-Caballero, M Montencino, Y-Xiong and HM Ryoo for reagents. We also thank E Adanero, E Castaño and B Torrejón for technical assistance. Natalia Artigas is the recipient of a fellowship from University of Barcelona. This research was supported by grants from the M.E.C. (BFU2014-56313-P) and La Marató de TV3.

1. Long F. Building strong bones: molecular regulation of the osteoblast lineage. *Nat Rev Mol Cell Biol* 2011; **13**: 27–38.
2. Karsenty G, Kronenberg HM, Settembre C. Genetic control of bone formation. *Annu Rev Cell Dev Biol* 2009; **25**: 629–648.
3. Sinha KM, Zhou X. Genetic and molecular control of osterix in skeletal formation. *J Cell Biochem* 2013; **114**: 975–984.
4. Ducy P, Zhang R, Geoffroy V, Ridall AL, Karsenty G. Osf2/Cbfa1: a transcriptional activator of osteoblast differentiation. *Cell* 1997; **89**: 747–754.
5. Zhou X, Zhang Z, Feng JQ, Dusevich VM, Sinha K, Zhang H *et al.* Multiple functions of Osterix are required for bone growth and homeostasis in postnatal mice. *Proc Natl Acad Sci USA* 2010; **107**: 12919–12924.
6. Baek WY, de Crombrugghe B, Kim JE. Postnatally induced inactivation of Osterix in osteoblasts results in the reduction of bone formation and maintenance. *Bone* 2010; **46**: 920–928.
7. Timpson NJ, Tobias JH, Richards JB, Soranzo N, Duncan EL, Sims AM *et al.* Common variants in the region around Osterix are associated with bone mineral density and growth in childhood. *Hum Mol Genet* 2009; **18**: 1510–1517.
8. Lapunzina P, Aglan M, Temtamy S, Caparros-Martin JA, Valencia M, Leton R *et al.* Identification of a frameshift mutation in Osterix in a patient with recessive osteogenesis imperfecta. *Am J Hum Genet* 2010; **87**: 110–114.
9. Artigas N, Urena C, Rodriguez-Carballo E, Rosa JL, Ventura F. Mitogen-activated protein kinase (MAPK)-regulated interactions between Osterix and Runx2 are critical for the transcriptional osteogenic program. *J Biol Chem* 2014; **289**: 27105–27117.
10. Hojo H, Ohba S, He X, Lai LP, McMahon AP. Sp7/osterix is restricted to bone-forming vertebrates where it acts as a Dlx co-factor in osteoblast specification. *Dev Cell* 2016; **37**: 238–253.
11. Ulsamer A, Ortuno MJ, Ruiz S, Susperregui AR, Osses N, Rosa JL *et al.* BMP-2 induces Osterix expression through up-regulation of Dlx5 and its phosphorylation by p38. *J Biol Chem* 2008; **283**: 3816–3826.
12. Ortuno MJ, Ruiz-Gaspa S, Rodriguez-Carballo E, Susperregui AR, Bartrons R, Rosa JL *et al.* p38 regulates expression of osteoblast-specific genes by phosphorylation of osterix. *J Biol Chem* 2010; **285**: 31985–31994.
13. Greenblatt MB, Shim JH, Zou W, Sitara D, Schweitzer M, Hu D *et al.* The p38 MAPK pathway is essential for skeletogenesis and bone homeostasis in mice. *J Clin Invest* 2010; **120**: 2457–2473.
14. Carvajal LA, Manfredi JJ. Another fork in the road–life or death decisions by the tumour suppressor p53. *EMBO Rep* 2013; **14**: 414–421.
15. Molchadsky A, Shats I, Goldfinger N, Pevsner-Fischer M, Olson M, Rinon A *et al.* p53 plays a role in mesenchymal differentiation programs, in a cell fate dependent manner. *PLoS ONE* 2008; **3**: e3707.
16. Liu H, Jia D, Li A, Chau J, He D, Ruan X *et al.* p53 regulates neural stem cell proliferation and differentiation via BMP-Smad1 signaling and Id1. *Stem Cells Dev* 2013; **22**: 913–927.
17. Wang X, Kua HY, Hu Y, Guo K, Zeng Q, Wu Q *et al.* p53 functions as a negative regulator of osteoblastogenesis, osteoblast-dependent osteoclastogenesis, and bone remodeling. *J Cell Biol* 2006; **172**: 115–125.
18. Armstrong JF, Kaufman MH, Harrison DJ, Clarke AR. High-frequency developmental abnormalities in p53-deficient mice. *Curr Biol* 1995; **5**: 931–936.
19. He Y, de Castro LF, Shin MH, Dubois W, Yang HH, Jiang S *et al.* p53 loss increases the osteogenic differentiation of bone marrow stromal cells. *Stem Cells* 2015; **33**: 1304–1319.
20. Ruan X, Zuo Q, Jia H, Chau J, Lin J, Ao J *et al.* P53 deficiency-induced Smad1 upregulation suppresses tumorigenesis and causes chemoresistance in colorectal cancers. *J Mol Cell Biol* 2015; **7**: 105–118.
21. Liu W, Qi M, Konermann A, Zhang L, Jin F, Jin Y. The p53/miR-17/Smurf1 pathway mediates skeletal deformities in an age-related model via inhibiting the function of mesenchymal stem cells. *Aging (Albany NY)* 2015; **7**: 205–218.
22. Ozaki T, Wu D, Sugimoto H, Nagase H, Nakagawara A. Runt-related transcription factor 2 (RUNX2) inhibits p53-dependent apoptosis through the collaboration with HDAC6 in response to DNA damage. *Cell Death Dis* 2013; **4**: e610.

23. van der Deen M, Taipaleenmaki H, Zhang Y, Teplyuk NM, Gupta A, Cinghu S *et al.* MicroRNA-34c inversely couples the biological functions of the runt-related transcription factor RUNX2 and the tumor suppressor p53 in osteosarcoma. *J Biol Chem* 2013; **288**: 21307–21319.
24. Lengner CJ, Steinman HA, Gagnon J, Smith TW, Henderson JE, Kream BE *et al.* Osteoblast differentiation and skeletal development are regulated by Mdm2-p53 signaling. *J Cell Biol* 2006; **172**: 909–921.
25. Nakashima K, Zhou X, Kunkel G, Zhang Z, Deng JM, Behringer RR *et al.* The novel zinc finger-containing transcription factor osterix is required for osteoblast differentiation and bone formation. *Cell* 2002; **108**: 17–29.
26. Ortuno MJ, Susperregui AR, Artigas N, Rosa JL, Ventura F. Osterix induces Col1a1 gene expression through binding to Sp1 sites in the bone enhancer and proximal promoter regions. *Bone* 2013; **52**: 548–556.
27. Yang Y, Huang Y, Zhang L, Zhang C. Transcriptional regulation of bone sialoprotein gene expression by Osx. *Biochem Biophys Res Commun* 2016; **476**: 574–579.
28. Chen H, Hays E, Liboon J, Neely C, Kolman K, Chandar N. Osteocalcin gene expression is regulated by wild-type p53. *Calcif Tissue Int* 2011; **89**: 411–418.
29. Chen H, Kolman K, Lanciloti N, Nerney M, Hays E, Robson C *et al.* p53 and MDM2 are involved in the regulation of osteocalcin gene expression. *Exp Cell Res* 2012; **318**: 867–876.
30. Chau JF, Jia D, Wang Z, Liu Z, Hu Y, Zhang X *et al.* A crucial role for bone morphogenetic protein-Smad1 signalling in the DNA damage response. *Nat Commun* 2012; **3**: 836.
31. Barbuto R, Mitchell J. Regulation of the osterix (Osx, Sp7) promoter by osterix and its inhibition by parathyroid hormone. *J Mol Endocrinol* 2013; **51**: 99–108.
32. Lee KS, Kim HJ, Li QL, Chi XZ, Ueta C, Komori T *et al.* Runx2 is a common target of transforming growth factor beta1 and bone morphogenetic protein 2, and cooperation between Runx2 and Smad5 induces osteoblast-specific gene expression in the pluripotent mesenchymal precursor cell line C2C12. *Mol Cell Biol* 2000; **20**: 8783–8792.
33. de Vries A, Flores ER, Miranda B, Hsieh HM, van Oostrom CT, Sage J *et al.* Targeted point mutations of p53 lead to dominant-negative inhibition of wild-type p53 function. *Proc Natl Acad Sci USA* 2002; **99**: 2948–2953.
34. Chen Y, Dey R, Chen L. Crystal structure of the p53 core domain bound to a full consensus site as a self-assembled tetramer. *Structure* 2010; **18**: 246–256.
35. Cho Y, Gorina S, Jeffrey PD, Pavletich NP. Crystal structure of a p53 tumor suppressor-DNA complex: understanding tumorigenic mutations. *Science* 1994; **265**: 346–355.
36. Kruiswijk F, Labuschagne CF, Vousden KH. p53 in survival, death and metabolic health: a lifeguard with a licence to kill. *Nat Rev Mol Cell Biol* 2015; **16**: 393–405.
37. Lee DF, Su J, Kim HS, Chang B, Papatsenko D, Zhao R *et al.* Modeling familial cancer with induced pluripotent stem cells. *Cell* 2015; **161**: 240–254.
38. Balboni AL, Cherukuri P, Ung M, DeCastro AJ, Cheng C, DiRenzo J. p53 and DeltaNp63alpha coregulate the transcriptional and cellular response to TGFbeta and BMP signals. *Mol Cancer Res* 2015; **13**: 732–742.
39. De Rosa L, Antonini D, Ferone G, Russo MT, Yu PB, Han R *et al.* p63 Suppresses non-epidermal lineage markers in a bone morphogenetic protein-dependent manner via repression of Smad7. *J Biol Chem* 2009; **284**: 30574–30582.
40. Roca H, Phimphilai M, Gopalakrishnan R, Xiao G, Franceschi RT. Cooperative interactions between RUNX2 and homeodomain protein-binding sites are critical for the osteoblast-specific expression of the bone sialoprotein gene. *J Biol Chem* 2005; **280**: 30845–30855.
41. Lee MH, Kim YJ, Yoon WJ, Kim JI, Kim BG, Hwang YS *et al.* Dlx5 specifically regulates Runx2 type II expression by binding to homeodomain-response elements in the Runx2 distal promoter. *J Biol Chem* 2005; **280**: 35579–35587.
42. Nishio Y, Dong Y, Paris M, O'Keefe RJ, Schwarz EM, Drissi H. Runx2-mediated regulation of the zinc finger Osterix/Sp7 gene. *Gene* 2006; **372**: 62–70.
43. Kawane T, Komori H, Liu W, Moriishi T, Miyazaki T, Mori M *et al.* Dlx5 and mef2 regulate a novel runx2 enhancer for osteoblast-specific expression. *J Bone Miner Res* 2014; **29**: 1960–1969.
44. Muller PA, Vousden KH. p53 mutations in cancer. *Nat Cell Biol* 2013; **15**: 2–8.
45. Vijayakumaran R, Tan KH, Miranda PJ, Haupt S, Haupt Y. Regulation of mutant p53 protein expression. *Front Oncol* 2015; **5**: 284.
46. Sui B, Hu C, Liao L, Chen Y, Zhang X, Fu X *et al.* Mesenchymal progenitors in osteopenias of diverse pathologies: differential characteristics in the common shift from osteoblastogenesis to adipogenesis. *Sci Rep* 2016; **6**: 30186.
47. Despars G, Carbonneau CL, Bardeau P, Coutu DL, Beausejour CM. Loss of the osteogenic differentiation potential during senescence is limited to bone progenitor cells and is dependent on p53. *PLoS ONE* 2013; **8**: e73206.
48. Velletri T, Xie N, Wang Y, Huang Y, Yang Q, Chen X *et al.* P53 functional abnormality in mesenchymal stem cells promotes osteosarcoma development. *Cell Death Dis* 2016; **7**: e2015.
49. Quist T, Jin H, Zhu JF, Smith-Fry K, Capecchi MR, Jones KB. The impact of osteoblastic differentiation on osteosarcomagenesis in the mouse. *Oncogene* 2015; **34**: 4278–4284.
50. Tang N, Song WX, Luo J, Haydon RC, He TC. Osteosarcoma development and stem cell differentiation. *Clin Orthop Relat Res* 2008; **466**: 2114–2130.
51. Walkley CR, Qudsi R, Sankaran VG, Perry JA, Gostissa M, Roth SI *et al.* Conditional mouse osteosarcoma, dependent on p53 loss and potentiated by loss of Rb, mimics the human disease. *Genes Dev* 2008; **22**: 1662–1676.
52. Muller PA, Vousden KH. Mutant p53 in cancer: new functions and therapeutic opportunities. *Cancer Cell* 2014; **25**: 304–317.
53. Kim MP, Zhang Y, Lozano G. Mutant p53: multiple mechanisms define biologic activity in cancer. *Front Oncol* 2015; **5**: 249.
54. Rodriguez-Carballo E, Ulsamer A, Susperregui AR, Manzanares-Cespedes C, Sanchez-Garcia E, Bartrons R *et al.* Conserved regulatory motifs in osteogenic gene promoters integrate cooperative effects of canonical Wnt and BMP pathways. *J Bone Miner Res* 2011; **26**: 718–729.
55. Gamez B, Rodriguez-Carballo E, Graupera M, Rosa JL, Ventura F. Class I PI-3-kinase signaling is critical for bone formation through regulation of SMAD1 activity in osteoblasts. *J Bone Miner Res* 2016; **31**: 1617–1630.
56. Ran FA, Hsu PD, Wright J, Agarwala V, Scott DA, Zhang F. Genome engineering using the CRISPR-Cas9 system. *Nat Protoc* 2013; **8**: 2281–2308.
57. Kitamura T, Koshino Y, Shibata F, Oki T, Nakajima H, Nosaka T *et al.* Retrovirus-mediated gene transfer and expression cloning: powerful tools in functional genomics. *Exp Hematol* 2003; **31**: 1007–1014.
58. Junk DJ, Vrba L, Watts GS, Oshiro MM, Martinez JD, Futscher BW. Different mutant/wild-type p53 combinations cause a spectrum of increased invasive potential in nonmalignant immortalized human mammary epithelial cells. *Neoplasia* 2008; **10**: 450–461.

Supplementary Information accompanies this paper on Cell Death and Differentiation website (http://www.nature.com/cdd)

References

Allalou, A. and Wählby, C. (2009). BlobFinder, a tool for fluorescence microscopy image cytometry. *Computer methods and programs in biomedicine*, 94(1):58–65.

Artigas, N., Gmez, B., Cubillos-Rojas, M., Snchez de Diego, C., Antonio Valer, J., Pons, G., Rosa, J. L., and Ventura, F. (2017). p53 inhibits SP7/Osterix activity in the transcriptional program of osteoblast differentiation.

Baek, J.-E., Choi, J.-Y., and Kim, J.-E. (2014). Skeletal analysis and differential gene expression in Runx2/Osterix double heterozygous embryos. *Biochemical and biophysical research communications*, 451(3):442–448.

Baek, W.-Y., Kim, Y.-J., de Crombrugghe, B., and Kim, J.-E. (2013). Osterix is required for cranial neural crest-derived craniofacial bone formation. *Biochemical and Biophysical Research Communications*, 432(1):188–192.

Barlow, J. L., Drynan, L. F., Hewett, D. R., Holmes, L. R., Lorenzo-Abalde, S., Lane, A. L., Jolin, H. E., Pannell, R., Middleton, A. J., Wong, S. H., et al. (2010). A p53-dependent mechanism underlies Macrocytic Anemia in a mouse model of human 5q-syndrome. *Nature medicine*, 16(1):59–66.

Berman, S. D., Calo, E., Landman, A. S., Danielian, P. S., Miller, E. S., West, J. C., Fonhoue, B. D., Caron, A., Bronson, R., Bouxsein, M. L., et al. (2008). Metastatic osteosarcoma induced by inactivation of Rb and p53 in the osteoblast lineage. *Proceedings of the National Academy of Sciences*, 105(33):11851–11856.

Boultwood, J., Pellagatti, A., and Wainscoat, J. S. (2012). Haploinsufficiency of ribosomal proteins and p53 activation in anemia: Diamond-Blackfan anemia and the 5q-syndrome. *Advances in biological regulation*, 52(1):196–203.

de Sousa Abreu, R., Penalva, L. O., Marcotte, E. M., and Vogel, C. (2009). Global signatures of protein and mrna expression levels. *Molecular BioSystems*, 5(12):1512–1526.

Fairus, A. M., Choudhary, B., Hosahalli, S., Kavitha, N., and Shatrah, O. (2017). Dihydroorotate dehydrogenase (DHODH) inhibitors affect ATP depletion, endogenous ROS and mediate S-phase arrest in breast cancer cells. *Biochimie*, 135:154–163.

Fang, J., Uchiumi, T., Yagi, M., et al. (2013). Dihydro-orotate dehydrogenase is physically associated with the Respiratory Complex and its loss leads to Mitochondrial Dysfunction. *Bioscience reports*, 33(2):e00021.

Fang, J., Uchiumi, T., Yagi, M., Matsumoto, S., Amamoto, R., Saito, T., Takazaki, S., Kanki, T., Yamaza, H., Nonaka, K., et al. (2012). Protein instability and functional defects caused by mutations of dihydro-orotate dehydrogenase in Miller syndrome patients. *Bioscience reports*, 32(6):631–639.

Fukushima, R., Kanamori, S., Hirashiba, M., Hishikawa, A., Muranaka, R.-i., Kaneto, M., and Kitagawa, H. (2009). Inhibiting the teratogenicity of the immunosuppressant leflunomide in mice by supplementation of exogenous uridine. *Toxicological sciences*, 108(2):419–426.

Gao, Y., Jheon, A., Nourkeyhani, H., Kobayashi, H., and Ganss, B. (2004). Molecular cloning, structure, expression, and chromosomal localization of the human Osterix (SP7) gene. *Gene*, 341:101–110.

Hail, N., Chen, P., Kepa, J. J., and Bushman, L. R. (2012). Evidence supporting a role for dihydroorotate dehydrogenase, bioenergetics, and p53 in selective teriflunomide-induced apoptosis in transformed versus normal human keratinocytes. *Apoptosis*, 17(3):258–268.

Inui, M., Miyado, M., Igarashi, M., Tamano, M., Kubo, A., Yamashita, S., Asahara, H., Fukami, M., and Takada, S. (2014). Rapid generation of mouse models with defined point mutations by the CRISPR/Cas9 system. *Scientific reports*, 4.

Jones, N. C., Lynn, M. L., et al. (2008). Prevention of the neurocristopathy Treacher Collins syndrome through inhibition of p53 function. *Nature medicine*, 14(2):125–133.

Kaback, L. A., Soung, D. Y., Naik, A., Smith, N., et al. (2008). Osterix/Sp7 regulates mesenchymal stem cell mediated endochondral ossification. *Journal of cellular physiology*, 214(1):173–182.

Karsenty, G., Kronenberg, H. M., and Settembre, C. (2009). Genetic control of bone formation. *Annual Review of Cell and Developmental*, 25:629–648.

Kato, T., Miyata, K., Sonobe, M., Yamashita, S., Tamano, M., Miura, K., Kanai, Y., Miyamoto, S., Sakuma, T., Yamamoto, T., et al. (2013). Production of Sry knockout mouse using TALEN via oocyte injection. *Scientific reports*, 3:3136.

Khutornenko, A. A., Roudko, V. V., et al. (2010). Pyrimidine biosynthesis links Mitochondrial Respiration to the p53 pathway. *Proceedings of the National Academy of Sciences*, 107(29):12828–12833.

Kuhn, R. M., Haussler, D., and Kent, W. J. (2012). The ucsc genome browser and associated tools. *Briefings in bioinformatics*, 14(2):144–161.

Lapunzina, P., Aglan, M., Temtamy, S., Caparrós-Martín, J. A., Valencia, M., Letón, R., Martínez-Glez, V., Elhossini, R., Amr, K., Vilaboa, N., et al. (2010). Identification of a frameshift mutation in Osterix in a patient with recessive Osteogenesis imperfecta. *The American Journal of Human Genetics*, 87(1):110–114.

Leban, J. and Vitt, D. (2011). Human dihydroorotate dehydrogenase inhibitors, a novel approach for the treatment of autoimmune and inflammatory diseases. *Arzneimittelforschung*, 61(01):66–72.

Levine, A. J. (1997). p53, the cellular gatekeeper for growth and division. *cell*, 88(3):323–331.

Linke, S. P., Clarkin, K. C., Di Leonardo, A., Tsou, A., and Wahl, G. M. (1996). A reversible, p53-dependent G0/G1 cell cycle arrest induced by Ribonucleotide Depletion in the absence of Detectable DNA Damage. *Genes & development*, 10(8):934–947.

Liu, L., Dong, Z., Lei, Q., Yang, J., Hu, H., Li, Q., Ji, Y., Guo, L., Zhang, Y., Liu, Y., et al. (2017). Inactivation/deficiency of DHODH induces cell cycle arrest and programed cell death in melanoma. *Oncotarget*, 5.

Miller, M., Fineman, R., and Smith, D. W. (1979). Postaxial Acrofacial Dysostosis Syndrome. *The Journal of pediatrics*, 95(6):970–975.

Mouse-Phenotype.

Ng, S. B., Buckingham, K. J., Lee, C., Bigham, A. W., et al. (2010). Exome sequencing identifies the cause of a Mendelian disorder. *Nature Genetics*, 42(1):30–35.

Ohyama, K., Chung, C., Chen, E., Gibson, C., Misof, K., Fratzl, P., and Shapiro, I. (1997). p53 influences mice skeletal development. *Journal of Craniofacial Genetics and Developmental Biology*, 17(4):161–171.

Ozaki, T., Wu, D., Sugimoto, H., Nagase, H., and Nakagawara, A. (2013). Runt-related transcription factor 2 (runx2) inhibits p53-dependent apoptosis through the collaboration with hdac6 in response to dna damage. *Cell death & disease*, 4(4):e610.

Piliszek, A., Kwon, G. S., and Hadjantonakis, A.-K. (2011). Ex utero culture and live imaging of mouse embryos. *Vertebrate Embryogenesis: Embryological, Cellular, and Genetic Methods*, pages 243–257.

Rainger, J., Bengani, H., Campbell, L., et al. (2012). Miller (GeneWiedemann) syndrome represents a Clinically and Biochemically distinct subgroup of Postaxial Acrofacial Dysostosis associated with partial deficiency of DHODH. *Human Molecular Genetics*, 21(18):3969–3983.

Ren, A., Fu, G., Qiu, Y., and Cui, H. (2017). Leflunomide inhibits proliferation and tumorigenesis of oral squamous cell carcinoma. *Molecular medicine reports*, 16(6):9125–9130.

Rinon, A., Molchadsky, A., Nathan, E., Yovel, G., Rotter, V., Sarig, R., and Tzahor, E. (2011). p53 coordinates Cranial Neural Crest Cell Growth and Epithelial-Mesenchymal transition/delamination processes. *Development*, 138(9):1827–1838.

Rueden, C. T., Schindelin, J., Hiner, M. C., DeZonia, B. E., Walter, A. E., Arena, E. T., and Eliceiri, K. W. (2017). ImageJ2: ImageJ for the next generation of scientific image data. *BMC bioinformatics*, 18(1):529.

Sakai, D., Dixon, J., Achilleos, A., Dixon, M., and Trainor, P. A. (2016). Prevention of Treacher Collins syndrome craniofacial anomalies in mouse models via maternal antioxidant supplementation. *Nature communications*, 7:10328.

Stoll, C., Dott, B., Roth, M.-P., and Alembik, Y. (1989). Birth prevalence rates of skeletal dysplasias. *Clinical genetics*, 35(2):88–92.

Takada, S., Sato, T., Ito, Y., Yamashita, S., Kato, T., Kawasumi, M., Kanai-Azuma, M., Igarashi, A., Kato, T., Tamano, M., et al. (2013). Targeted gene deletion of miRNAs in mice by TALEN system. *PLoS One*, 8(10):e76004.

Tang, W., Li, Y., Osimiri, L., and Zhang, C. (2011). Osteoblast-specific transcription factor osterix (osx) is an upstream regulator of satb2 during bone formation. *Journal of Biological Chemistry*, 286(38):32995–33002.

Thymiakou, E. and Episkopou, V. (2011). Detection of signaling effector-complexes downstream of BMP4 using in situ PLA, a proximity ligation assay. *Journal of visualized experiments: JoVE*, (49).

Tian, Y., Xu, Y., Fu, Q., and Dong, Y. (2012). Osterix is required for Sonic hedgehog-induced osteoblastic MC3T3-E1 cell differentiation. *Cell biochemistry and biophysics*, 64(3):169–176.

Ueda, Y., Okano, M., Williams, C., Chen, T., Georgopoulos, K., and Li, E. (2006). Roles for Dnmt3b in mammalian development: a mouse model for the ICF syndrome. *Development*, 133(6):1183–1192.

Vélez, J., Hail Jr, N., Konopleva, M., Zeng, Z., Kojima, K., Samudio, I., and Andreeff, M. (2013). Mitochondrial uncoupling and the reprograming of intermediary metabolism in leukemia cells. *Frontiers in oncology*, 3.

Wang, X., Kua, H.-Y., Hu, Y., Guo, K., Zeng, Q., Wu, Q., Ng, H.-H., Karsenty, G., de Crombrugghe, B., Yeh, J., et al. (2006). p53 functions as a negative regulator of osteoblastogenesis, osteoblast-dependent osteoclastogenesis, and bone remodeling. *J Cell Biol*, 172(1):115–125.

White, R. M., Cech, J., Ratanasirintrawoot, S., Lin, C. Y., Rahl, P. B., Burke, C. J., Langdon, E., Tomlinson, M. L., Mosher, J., Kaufman, C., et al. (2011). DHODH modulates transcriptional elongation in the neural crest and melanoma. *Nature*, 471(7339):518–522.

Zhang-Laboratories. *CRISPR Design*. http://crispr.mit.edu/, [Accessed: 15 January 2018].